

Electronic structure of 3d-transition-metal monoxide anions from GW calculations: ScO^- , TiO^- , CuO^- , and ZnO^-

Young-Moo Byun and Serdar Ögüt¹

¹*Department of Physics, University of Illinois at Chicago, Chicago, IL 60607, USA*

The GW approximation to many-body perturbation theory is a reliable tool for describing charged electronic excitations, and it has been successfully applied to a wide range of extended systems for several decades using a plane-wave basis. However, the GW approximation has been used to test limited spectral properties of a limited set of finite systems (e.g. frontier orbital energies of closed-shell sp molecules) only for about a decade using a local-orbital basis. Here, we calculate the quasiparticle spectra of closed- and open-shell molecular anions with partially and completely filled 3d shells (i.e. with shallow and deep 3d states), ScO^- , TiO^- , CuO^- , and ZnO^- , using various levels of GW theory, and compare them to experiments to evaluate the performance of the GW approximation on the electronic structure of small molecules containing 3d transition metals. We find that the G -only eigenvalue-only self-consistent GW scheme with W fixed to the PBE level ($G_nW_0\text{@PBE}$), which gives the best compromise between accuracy and efficiency for solids, also gives good results for both localized (d) and delocalized (sp) states of transition metal oxide molecules. The success of $G_nW_0\text{@PBE}$ in predicting electronic excitations in these systems reasonably well is likely due to the fortuitous cancellation effect between the overscreening of the Coulomb interaction by PBE and the underscreening by the neglect of vertex corrections. Together with the absence of the self-consistent field convergence error (e.g. due to spin contamination in open-shell systems) and the GW multi-solution issue, the $G_nW_0\text{@PBE}$ scheme gives the possibility to predict the electronic structure of complex real systems (e.g. molecule-solid and $sp-d$ hybrid systems) accurately and efficiently.

I. INTRODUCTION

It is a challenging task to accurately determine the electronic structure of an interacting many-electron system. In experiment, electron removal and addition energies of both extended and finite systems are measured by direct and inverse photoelectron spectroscopy (PES and IPES, respectively). In theory, it is well known that the GW approximation to many-body perturbation theory (MBPT) describes bandgaps and band structures of solids more accurately than local and semi-local approximations to density-functional theory (DFT).^{1,2} However, less is known about the performance of the GW approximation on the electronic structure of atoms, molecules, and clusters. Especially, GW calculations for the quasiparticle (QP) spectra of open-shell molecules containing 3d transition metals are scarce. There are a few reasons for it.

First, it is easier to test only frontier orbital energies such as the ionization energy (IE) and the electron affinity (EA) than the full QP spectrum (all orbital energies). There are mainly two ways to calculate IE and EA of molecules. On one hand, IE (EA) can be obtained from the DFT, HF (Hartree-Fock), MP2 (second-order Møller-Plesset perturbation theory), RPA (random-phase approximation), or CCSD(T) (coupled-cluster singles and doubles plus perturbative triples) total energy differences between a neutral and a cation (anion) within the so-called ΔSCF (self-consistent field) method.³ Generally, the ΔSCF method gives accurate frontier orbital energies of molecules and small clusters, but it does not work for solids and large clusters, and cannot access the full QP spectrum. On the other hand, IE and EA can be

obtained from GW eigenvalues for the HOMO (highest occupied molecular orbital) and the LUMO (lowest occupied molecular orbital), respectively. Due to the simplicity of the ΔSCF method, many studies have evaluated the performance of the GW approximation on molecules only by comparing GW IE and EA to ΔSCF ones,⁴ but that approach does not utilize the full power of the GW approximation, which is the ability to provide the QP spectrum for both finite and extended systems. For example, Bethe-Salpeter equation (BSE) calculations for the study of optical excitations require more orbital energies than IE and EA as input.⁵

Second, it is easier to test closed-shell systems than open-shell ones. Most of quantum-chemistry-based GW implementations for finite systems, such as MOLGW,⁶ FIESTA,⁷ TURBOMOLE,⁸ FHI-AIMS,³ and CP2K,⁹ use local-orbital basis sets such as Gaussian basis sets. GW calculations require mean-field self-consistent calculations, such as restricted and unrestricted Hartree-Fock or Kohn-Sham (RHF or RKS and UHF or UKS, respectively) calculations for closed- and open-shell systems, respectively. The problem is that unlike RHF and RKS self-consistent calculations, UHF and UKS ones are not guaranteed to converge, as their convergence strongly depends on the initial guess wavefunctions. This is especially the case for spin-unrestricted calculations performed with hybrid exchange-correlation (xc) functionals, which include a fraction of exact exchange (EXX), and HF on 3d-transition-metal-containing molecules.^{10,11} Partially due to this SCF convergence issue, most existing studies have used only closed-shell systems to assess the performance of the GW approximation on finite systems. For example, Refs. 12–15 used the so-called

*GW*100 benchmark set, which is composed of only closed-shell molecules.

Last, it is easier to test *sp*-electron systems than *d*-electron ones. Fundamentally, it is more difficult to accurately predict the electronic structure of *d* systems (especially, 3*d* systems) than *sp* ones because of the strong localization, and thus the strong correlation, of *d* electrons. For example, it is challenging for *GW* to accurately reproduce bandgaps and *d*-band positions of bulk ZnO at the same time.^{16–18} Practically, it is computationally more demanding to tackle systems with *d*-electrons than those with only *sp*-electrons. For example, *d* elements have more basis functions than *sp* ones, which increases the computational costs, and transition-metal-containing molecules, especially with partially filled *d* shells and low multiplicity states, aggravate the above-mentioned SCF convergence issue, which makes it necessary to test many initial guess wavefunctions to ascertain the convergence of mean-field self-consistent calculations.

The *GW* approximation is unique, but the *GW* flavor is not. Due to the high computational cost of the *GW* approximation, there are many different types of *GW* schemes and variants. Generally, there are two approaches. One approach is to vary the self-consistency level in the *GW* approximation. The *GW* self-consistent levels from the lowest to the highest include the perturbative non-self-consistent (one-shot) *GW* (G_0W_0) scheme, the eigenvalue-only self-consistent *GW* (ev*GW*) scheme (with two types G_nW_0 and G_nW_n , which update eigenvalues only in *G* and in both *G* and *W*, respectively), the QP self-consistent *GW* (QSGW) scheme using a static and Hermitian approximation to the *GW* self-energy, and the fully self-consistent *GW* (SCGW) scheme.¹ Generally, as the *GW* self-consistency level increases, the *GW* approximation depends less on the mean-field starting point and becomes more conserving with respect to particle number, momentum, and energy. However, the higher *GW* self-consistency level does not necessarily give more accurate QP energies because vertex corrections are missing in the *GW* approximation. For example, SCGW and QSGW systematically overestimate the bandgaps of solids,¹⁹ displaying worse performance than ev*GW*, which currently provides the best balance between accuracy and efficiency for solids.¹⁶

The other approach is to vary the amount of EXX in the *GW* starting point to reduce the self-interaction error by semi-local xc functionals. When used within the G_0W_0 scheme, this approach is efficient, because unlike self-consistent *GW*, G_0W_0 performs computationally demanding self-energy calculations just once only for states of interest. However, the predictive power of this approach is questionable, since the optimal amount of EXX in the *GW* starting point is strongly system-dependent. For example, for extended systems, the reported values for the optimal amount of EXX are narrowly spread between 0% and 25%,¹⁷ while for finite systems, they are widely spread between 25% and 100%.^{4,20–22}

The purpose of this work is to evaluate the perfor-

mance of the *GW* approximation on the electronic structure of small oxide molecules containing 3*d* transition metals. To this end, we calculate the QP spectra of closed- and open-shell molecular anions with partially and completely filled 3*d* shells, ScO^- , TiO^- , CuO^- , and ZnO^- , using various levels of *GW* theory. There are a few reasons why we chose these molecular systems: (i) their anion PES data is available,^{23–26} (ii) CuO^- and ZnO^- are molecular analogs to bulk Cu_2O and ZnO , respectively, which are challenging systems for the *GW* method,^{27,28} and (iii) shallow and deep 3*d* states are measured in TiO^- and CuO^- , respectively.

This article is organized as follows: First, we give a brief introduction to the *GW* approximation and its implementation in the framework of quantum chemistry. Second, we present various convergence test results and show that care should be taken to obtain reliable and reproducible QP energies of finite systems from Gaussian-based *GW* implementations. Third, we assess various *GW* schemes, focusing on ionization energies and 3*d*-electron binding energies. We conclude that the G_nW_0 @PBE scheme gives the best performance among *GW* schemes considered in this work in terms of accuracy and efficiency. Last, we discuss the origin of seemingly conflicting *GW* results for finite systems in the literature.

II. THEORETICAL BACKGROUND

In this section, we briefly review the *GW* approximation and its implementation using local-orbital basis sets. This section contains only a minimal number of equations, which will be needed later. More details can be found in Refs. 6, 8, 12, and 29. Generally, we follow the notation in the MOLGW implementation paper and source code for consistency:⁶ (i) Hartree atomic units are used in all equations, (ii) The complex conjugate notation is not used for wavefunctions, because they are real in finite systems, (iii) State indices *i* and *j* run over only occupied states, *a* and *b* run over only empty (virtual) states, and *m* and *n* run over all states, (iv) The response function is referred to as the polarizability instead of the susceptibility, and (v) χ is used for the polarizability instead of *P* and Π .

A. *GW* Approximation

In Hedin's *GW* approximation, which neglects vertex corrections, the non-local, dynamical, and non-Hermitian self-energy Σ^σ at frequency ω is given by

$$\Sigma^\sigma(\mathbf{r}, \mathbf{r}', \omega) = \frac{i}{2\pi} \int d\omega' e^{i\eta\omega'} G^\sigma(\mathbf{r}, \mathbf{r}', \omega + \omega') W(\mathbf{r}', \mathbf{r}, \omega'), \quad (1)$$

where σ is the spin channel (\uparrow or \downarrow), G^σ is the time-ordered (causal) one-particle Green's function, *W* is the dynamically screened Coulomb interaction, and η is a positive infinitesimal.

The self-energy in Eq. (1) can be calculated from first principles by solving the coupled Hedin's equations in order. One starts by constructing the one-particle Green's function using the one-electron energy eigenvalues ϵ_m^σ and the corresponding wavefunctions $\varphi_m^\sigma(\mathbf{r})$ obtained from the Hartree or some other mean-field approximation:

$$G^\sigma(\mathbf{r}, \mathbf{r}', \omega) = \sum_i \frac{\varphi_i^\sigma(\mathbf{r})\varphi_i^\sigma(\mathbf{r}')}{\omega - \epsilon_i^\sigma - i\eta} + \sum_a \frac{\varphi_a^\sigma(\mathbf{r})\varphi_a^\sigma(\mathbf{r}')}{\omega - \epsilon_a^\sigma + i\eta}, \quad (2)$$

where i runs over occupied states and a runs over empty states. Note that G^σ in Eq. (2) is not the interacting (dressed) Green's function, but the non-interacting (bare) one. Conventionally, they are denoted by G^σ and G_0^σ , respectively, and related by the Dyson equation: $G^\sigma = G_0^\sigma + G_0^\sigma \Delta \Sigma^\sigma G^\sigma$. In this work, we use the subscript 0 to distinguish the non-self-consistent GW method from the self-consistent one.

Using the one-particle Green's function in Eq. (2), one can successively obtain the non-interacting polarizability χ_0 and the interacting polarizability $\chi = \chi_0[1 - v\chi_0]^{-1}$ within the random-phase approximation (RPA), the screened Coulomb interaction, and the self-energy:

$$\chi_0 = -i \sum_\sigma G^\sigma G^\sigma, \quad (3)$$

$$W = v + v\chi_0 W = v + v\chi_0 v + v\chi_0 v\chi_0 v + \dots = v + v\chi v, \quad (4)$$

$$\Sigma^\sigma = iG^\sigma W = iG^\sigma(v + v\chi v) = \Sigma_x^\sigma + \Sigma_c^\sigma, \quad (5)$$

where v denotes the bare Coulomb interaction $v(\mathbf{r}, \mathbf{r}') = 1/|\mathbf{r} - \mathbf{r}'|$, Σ_x is the exchange part of the self-energy, and Σ_c is the correlation part of the self-energy. Note that in Eqs. (3), (4), and (5), space and frequency variables $(\mathbf{r}, \mathbf{r}', \omega)$ are omitted for simplicity, and $\chi_0(\omega)$, $\chi(\omega)$, $\Sigma^\sigma(\omega)$, and $\Sigma_c^\sigma(\omega)$ are dynamic, whereas v and Σ_x^σ are static.

Using the real part of the self-energy in Eq. (5) and the first-order perturbation theory, one can obtain the (diagonal) QP equation:

$$\epsilon_m^{\text{G}_0\text{W}_0, \sigma} = \epsilon_m^\sigma + \langle \varphi_m^\sigma | \text{Re} \Sigma^\sigma(\epsilon_m^{\text{G}_0\text{W}_0, \sigma}) - v_{\text{xc}}^\sigma | \varphi_m^\sigma \rangle, \quad (6)$$

where $\epsilon_m^{\text{G}_0\text{W}_0, \sigma}$ are the perturbative one-shot GW QP energies and v_{xc}^σ is the exchange-correlation (xc) potential. The effect of off-diagonal elements of the self-energy on QP energies is not studied in this work. Experimentally, $\epsilon_m^{\text{G}_0\text{W}_0, \sigma}$ correspond to vertical IEs and EAs in PES and IPES, respectively. Theoretically, $\epsilon_m^{\text{G}_0\text{W}_0, \sigma}$ correspond to the positions of poles of the Green's function in the spectral (Lehmann) representation and thereby to the positions of QP peaks and plasmon satellites in the corresponding spectral function A^σ :

$$A_{mm}^\sigma(\mathbf{r}, \mathbf{r}', \omega) = \frac{1}{\pi} |\text{Im} G_{mm}^\sigma(\mathbf{r}, \mathbf{r}', \omega)|, \quad (7)$$

where A_{mm}^σ are the diagonal elements of the spectral function, G_{mm}^σ are the diagonal elements of the Green's function, and Im represents the imaginary part.

G^σ in Eq. (7) is the interacting Green's function, whereas G^σ in Eq. (2) is the non-interacting one. In other words, by plugging G^σ in Eq. (2) into Eq. (7) after replacing ϵ_m^σ , where $m = i$ or a , by $\epsilon_m^\sigma + \langle \varphi_m^\sigma | \Sigma^\sigma(\omega) - v_{\text{xc}}^\sigma | \varphi_m^\sigma \rangle$, one can find that A_{mm}^σ have peaks at

$$\omega = \epsilon_m^\sigma + \langle \varphi_m^\sigma | \text{Re} \Sigma^\sigma(\omega) - v_{\text{xc}}^\sigma | \varphi_m^\sigma \rangle, \quad (8)$$

which shows that solving the QP equation in Eq. (6) and locating the peak positions in the spectral function in Eq. (7) are equivalent ways of obtaining the QP energies.

The QP equation in Eq. (6) is non-linear, because Σ^σ depends on $\epsilon_m^{\text{G}_0\text{W}_0, \sigma}$, so it should be solved numerically. Additionally, Hedin equations are coupled, because W and Σ^σ depend on G^σ , so they should be solved self-consistently. Multiple ways to numerically solve the non-linear QP equation and to iteratively solve the coupled Hedin equations will be discussed later.

B. Self-Consistent Field Method

In order to obtain the ingredients for the one-particle Green's function in Eq. (2) using local-orbital basis sets, molecular orbitals (MOs) and corresponding MO energies are used as one-electron wavefunctions and corresponding eigenvalues. MOs are expanded as a linear combination of atomic orbitals (AOs) ϕ_μ :

$$\varphi_m^\sigma(\mathbf{r}) = \sum_\mu C_{\mu m}^\sigma \phi_\mu(\mathbf{r}), \quad (9)$$

where $C_{\mu m}^\sigma$ are MO expansion coefficients. In MOLGW, atom-centered (contracted) Gaussian orbitals are used as AOs.

The MO coefficients in Eq. (9) and MO energies can be obtained by solving the generalized Kohn-Sham (gKS) equation (i.e. the Hartree-Fock-Kohn-Sham scheme³⁰ for (semi-)local functionals, hybrid functionals, and HF):

$$\mathbf{H}^\sigma \mathbf{C}^\sigma = \mathbf{S} \mathbf{C}^\sigma \epsilon^\sigma, \quad (10)$$

where \mathbf{C}^σ is a matrix of MO coefficients, ϵ^σ is a diagonal matrix of MO energies, \mathbf{S} is the AO overlap matrix with elements:

$$S_{\mu\nu} = \int d\mathbf{r} \phi_\mu(\mathbf{r}) \phi_\nu(\mathbf{r}), \quad (11)$$

and \mathbf{H}^σ is the Hamiltonian matrix with elements:

$$H_{\mu\nu}^\sigma = T_{\mu\nu} + V_{\text{ext}, \mu\nu} + J_{\mu\nu} - \alpha K_{\mu\nu}^\sigma + (1-\alpha) V_{\text{x}, \mu\nu}^{\text{PBE}, \sigma} + V_{\text{c}, \mu\nu}^{\text{PBE}, \sigma}, \quad (12)$$

where T , V_{ext} , J , and K^σ are the kinetic energy, external potential energy, Hartree, and Fock exchange terms, respectively, V_{x}^σ and V_{c}^σ are the exchange and correlation potentials, respectively, and α is the fraction of EXX in the hybrid functionals that we refer to as PBE α in this work.

We briefly explain only a few terms in the Hamiltonian matrix in Eq. (12), which will be needed later. The matrix elements of the Hartree term in Eq. (12) are given by

$$J_{\mu\nu} = \sum_{\lambda\tau} (\mu\nu|\lambda\tau) \sum_{\sigma} D_{\lambda\tau}^{\sigma}, \quad (13)$$

where $(\mu\nu|\lambda\tau)$ are the 4-center two-electron Coulomb repulsion integrals:

$$(\mu\nu|\lambda\tau) = \iint d\mathbf{r}d\mathbf{r}' \phi_{\mu}(\mathbf{r})\phi_{\nu}(\mathbf{r}) \frac{1}{|\mathbf{r}-\mathbf{r}'|} \phi_{\lambda}(\mathbf{r}')\phi_{\tau}(\mathbf{r}'), \quad (14)$$

and \mathbf{D}^{σ} is the density matrix with elements:

$$D_{\mu\nu}^{\sigma} = \sum_m f_m^{\sigma} C_{\mu m}^{\sigma} C_{\nu m}^{\sigma}, \quad (15)$$

where f^{σ} is the occupation number (0 or 1). The matrix elements of the Fock exchange term in Eq. (12) are given by

$$K_{\mu\nu}^{\sigma} = \sum_{\lambda\tau} D_{\lambda\tau}^{\sigma} (\mu\lambda|\tau\nu). \quad (16)$$

The exchange and correlation potentials in Eq. (12) depend on the density ρ^{σ} (and the density gradient $\nabla\rho^{\sigma}$):

$$\rho^{\sigma}(\mathbf{r}) = \sum_{\mu\nu} D_{\mu\nu}^{\sigma} \phi_{\mu}(\mathbf{r})\phi_{\nu}(\mathbf{r}). \quad (17)$$

The gKS equation in Eq. (10) (i.e. the restricted Roothaan-Hall or unrestricted Pople-Nesbet equations) should be solved using the SCF method, because J , K^{σ} , V_x^{σ} , and V_c^{σ} in Eq. (12) depend on the density matrix in Eq. (15), as shown in Eqs. (13), (16), and (17).

C. GW Self-Energy

In order to obtain the ingredients for the interacting polarizability in Eq. (4), one should solve the Casida equation:

$$\begin{pmatrix} \mathbf{A} & \mathbf{B} \\ -\mathbf{B} & -\mathbf{A} \end{pmatrix} \begin{pmatrix} X^s \\ Y^s \end{pmatrix} = \Omega_s \begin{pmatrix} X^s \\ Y^s \end{pmatrix}, \quad (18)$$

where \mathbf{A} and \mathbf{B} are the resonant and coupling matrices, respectively, and the eigenvalues Ω_s are the neutral two-particle excitation energies. The matrix elements in \mathbf{A} and \mathbf{B} are given by

$$A_{ia\sigma}^{jb\sigma'} = (\epsilon_a^{\sigma} - \epsilon_i^{\sigma}) \delta_{ij} \delta_{ab} \delta_{\sigma\sigma'} + (ia\sigma|jb\sigma') + f_{xc,ia\sigma}^{jb\sigma'}, \quad (19)$$

$$B_{ia\sigma}^{jb\sigma'} = (ia\sigma|bj\sigma') + f_{xc,ia\sigma}^{bj\sigma'}, \quad (20)$$

where i and j are for occupied states, a and b are for empty states, f_{xc} is the time-dependent density-functional theory (TDDFT) xc kernel, and $(ia\sigma|jb\sigma')$ are the 4-orbital two-electron Coulomb repulsion integrals:

$$(ia\sigma|jb\sigma') = \iint d\mathbf{r}d\mathbf{r}' \varphi_i^{\sigma}(\mathbf{r})\varphi_a^{\sigma}(\mathbf{r}) \frac{1}{|\mathbf{r}-\mathbf{r}'|} \varphi_j^{\sigma'}(\mathbf{r}')\varphi_b^{\sigma'}(\mathbf{r}'). \quad (21)$$

In this work, we used the RPA by setting $f_{xc} = 0$, unlike in Ref. 8, where W is obtained with TDDFT screening (TDDFT and RPA polarizabilities make a difference of ~ 0.1 eV in the G_0W_0 @PBE QP energy for HOMO). The MO integrals in Eq. (21) are transformed from the AO integrals in Eq. (14) through the AO-MO integral transformation:

$$(ia\sigma|jb\sigma') = \sum_{\mu\nu\lambda\tau} C_{\mu i}^{\sigma} C_{\nu a}^{\sigma} C_{\lambda j}^{\sigma'} C_{\tau b}^{\sigma'} (\mu\nu|\lambda\tau), \quad (22)$$

which scales as $O(N^5)$ with N being the system size. Note that this integral transformation is a bottleneck in both Gaussian-based GW and MP2 calculations.

Diagonalizing the Casida-equation matrix in Eq. (18) yields eigenvalues Ω_s and eigenvectors (X^s, Y^s) . In MOLGW, the diagonalization is performed without using the Tamm-Dancoff approximation (TDA), which sets \mathbf{B} to zero, but efficiently using the so-called beyond-TDA method as shown in Refs. 6, 31, and 32. Using Ω_s and (X^s, Y^s) , one can construct the spectral representation of the interacting polarizability $\chi(\omega)$ as shown in Refs. 8, 12, and 29. From $\chi(\omega)$ and Eq. (4), one can obtain the spectral representation of the screened Coulomb interaction $W(\omega)$ as shown in Refs. 6, 8, 12, and 29. Using $W(\omega)$ and Eq. (5), and analytically performing the convolution of $G^{\sigma}(\omega)$ and $W(\omega)$ in the frequency domain, one can obtain the exchange and correlation parts of the GW self-energy Σ_x^{σ} and $\Sigma_c^{\sigma}(\omega)$, respectively, whose diagonal matrix elements are given by

$$\langle \varphi_m^{\sigma} | \Sigma_x^{\sigma} | \varphi_m^{\sigma} \rangle = - \sum_i (m i \sigma | i m \sigma), \quad (23)$$

$$\begin{aligned} \langle \varphi_m^{\sigma} | \Sigma_c^{\sigma}(\omega) | \varphi_m^{\sigma} \rangle &= \sum_{is} \frac{w_{m i \sigma}^s w_{m i \sigma}^s}{\omega - \epsilon_i^{\sigma} + \Omega_s - i\eta}, \\ &+ \sum_{as} \frac{w_{m a \sigma}^s w_{m a \sigma}^s}{\omega - \epsilon_a^{\sigma} - \Omega_s + i\eta}, \end{aligned} \quad (24)$$

where i runs over occupied states, a runs over empty states, s runs over all excitations, and $w_{mn\sigma}^s$ are given by

$$w_{mn\sigma}^s = \sum_{ia\sigma'} (m n \sigma | i a \sigma') (X_{ia\sigma'}^s + Y_{ia\sigma'}^s). \quad (25)$$

Note that unlike the plasmon-pole approximation (PPA), the analytic continuation method, and the contour deformation technique, the fully analytic method employed in RGWBS,²⁹ TURBOMOLE, and MOLGW gives the exact GW self-energy at all frequency points because it does not rely on any approximation and numerical parameter.^{12,33}

D. Spin Contamination

In unrestricted Hartree-Fock and Kohn-Sham calculations for open-shell systems, the expectation value of the

total angular momentum $\langle S^2 \rangle$ is given by

$$\langle S^2 \rangle = S(S+1) + N_\downarrow - \sum_i \sum_j^{N_\uparrow, N_\downarrow} |\langle \varphi_i^\uparrow | \varphi_j^\downarrow \rangle|^2, \quad (26)$$

where N_\uparrow and N_\downarrow are the numbers of \uparrow - and \downarrow -spin electrons, respectively, and S is $(N_\uparrow - N_\downarrow)/2$ with $N_\uparrow > N_\downarrow$. The last two terms on the right side of Eq. (26) are called the spin contamination, which is non-negative.^{34,35} The spin contamination becomes large when a ground state is mixed with (i.e. contaminated by) excited states.

In restricted calculations for closed-shell systems, the SCF cycle always converges to a global minimum and the spin contamination is zero for all (semi-)local and hybrid functionals as well as HF. In unrestricted calculations for open-shell systems, the SCF convergence and the spin contamination depend on the amount of EXX and the size of basis. For (semi-)local functionals, the SCF cycle almost always converges to a global minimum and the spin contamination is small [generally smaller than $\sim 10\%$ of $S(S+1)$]. For hybrid functionals and HF, there is a chance (which increases with EXX amount and basis size) that the SCF cycle does not converge or converges to local minima and the spin contamination is large.

Note that the spin contamination is just an indicator for the SCF convergence error, therefore, a small spin contamination does not guarantee the successful and correct convergence of the SCF cycle. Note also that the spin contamination generally raises, but sometimes lowers the gKS total energy, so the lowest gKS total energy does not guarantee the successful and correct convergence of the SCF cycle, either. In other words, the spin contamination and the gKS total energy are only two of multiple indicators for the evaluation of the convergence of the SCF cycle in unrestricted calculations with hybrid functionals and HF.

E. Auxiliary Basis Sets and Parallelization

In Gaussian-based *GW*, the 4-center integrals $(\mu\nu|\lambda\tau)$ in Eq. (14), which scale as $O(N^4)$, are a bottleneck in both gKS and *GW* calculations in terms of time and memory. The resolution-of-identity (RI) approximation is a method to address this issue by expanding the product of basis functions $\phi_\mu(\mathbf{r})\phi_\nu(\mathbf{r})$ as a linear combination of auxiliary basis functions $\phi_P(\mathbf{r})$.^{3,36,37} There are two types of the RI approximation: RI-V using a Coulomb metric and RI-SVS using an overlap metric. FIESTA uses both RI-V and RI-SVS, whereas MOLGW uses only RI-V, which is known to be superior to RI-SVS. Within RI-V, the 4-center integrals $(\mu\nu|\lambda\tau)$ in Eq. (14) approximate to

$$(\mu\nu|\lambda\tau) \approx \sum_{PQ} (\mu\nu|P)(P|Q)^{-1}(Q|\lambda\tau), \quad (27)$$

where P and Q run over auxiliary basis functions, $(\mu\nu|P)$ and $(Q|\lambda\tau)$ are the 3-center integrals, and $(P|Q)$ are the

2-center integrals.

RI can be applied to both gKS (i.e. J and K^σ) and *GW* [i.e. \mathbf{A} , \mathbf{B} , Σ_x^σ , and $\Sigma_c^\sigma(\omega)$] calculations. In this work, we refer to RI applied to one (both) of them as a half (full) RI method. For example, FIESTA uses a half RI method, whereas MOLGW uses a full RI method. In this work, we observed that a full RI method in MOLGW reduces computational costs in terms of both time and memory by about the number of basis functions, i.e. by ~ 100 - 300 times, as shown in Table I.

RI is an approximation, so it causes an error. There are mixed results for the RI error in the literature, ranging from ~ 1 meV to ~ 0.1 eV, because different molecular systems, molecular orbitals, levels of theory (DFT vs *GW*), xc functionals (PBE vs HF), and basis sets are used to evaluate the quality of RI.^{12,20} RI should be used only after careful and thorough tests.

In order to reduce the high computational and memory cost of the 4-center integrals $(\mu\nu|\lambda\tau)$ in Eq. (14), we parallelized the 4-center integrals in Eqs. (13), (16), (19), (20), (22), (23), (24), and (25) using Open Multi-Processing (OpenMP), which consumes much less memory than Message Passing Interface by using shared-memory threads. The performance gain by our OpenMP implementation is shown in the supplementary material. We also optimized our OpenMP implementation to reduce Non-Uniform Memory Access (NUMA) effects in modern multi-core processors by enhancing the memory bandwidth and reducing the memory latency. Our OpenMP implementation in MOLGW 1.F has recently been merged into MOLGW 2.A.

F. G_0W_0 Quasiparticle Energy

In this work, we used three methods to obtain $\epsilon_m^{G_0W_0}$, as it is practically impossible to obtain $\epsilon_m^{G_0W_0}$ accurately for all energy levels of all molecular systems using a single method, which will be discussed in detail later. Note that in the following, the spin channel σ and the real part Re are omitted for simplicity.

The first method is to linearize the non-linear QP equation in Eq. (6):

$$\epsilon_m^{G_0W_0} \approx \epsilon_m + Z_m^{\text{linear}} \langle \varphi_m | \Sigma(\epsilon_m) - v_{\text{xc}} | \varphi_m \rangle \equiv \epsilon_m^{G_0W_0, \text{linear}}, \quad (28)$$

where $\epsilon_m^{G_0W_0, \text{linear}}$ is the perturbative one-shot QP energy obtained from the linearization, and Z_m^{linear} is the QP renormalization factor for the linearization:

$$Z_m^{\text{linear}} = \frac{1}{1 - \frac{\partial}{\partial \omega} \langle \varphi_m | \Sigma(\omega) | \varphi_m \rangle |_{\omega=\epsilon_m}}, \quad (29)$$

where the derivative of the self-energy is obtained from the finite difference method using two frequency points at $\epsilon_m \pm \Delta\omega$ with $\Delta\omega$ being the frequency grid spacing, which is set to 0.001 Ha in this work.

There are a few points to note about the linearization method. First, one can choose different frequency points

for the finite difference method (e.g. $\epsilon_m \pm 0.1$ eV and $\epsilon_m \pm 0.5$ eV in Refs. 14 and 38, respectively). In the plasmon-pole approximation (PPA) G_0W_0 method, different frequency points give similar results for $\epsilon_m^{G_0W_0, \text{linear}}$, because PPA makes $\langle \varphi_m | \Sigma_c(\omega) | \varphi_m \rangle$ in Eq. (24) smooth around ϵ_m by drastically reducing the number of self-energy poles.³⁸ However, in the full-frequency G_0W_0 method, different frequency points can give very different results for $\epsilon_m^{G_0W_0, \text{linear}}$ when the finite difference method fails due to weak self-energy poles around ϵ_m , which will be discussed later. Second, the derivative of the self-energy can be evaluated analytically as shown in Ref. 8, but it is not used in this work. Last, Z_m^{linear} in Eq. (29) is slightly different from that in Ref. 12, $Z_m^{\text{GW100}} = 1/[1 - (\partial/\partial\omega)\langle \varphi_m | \Sigma(\omega) | \varphi_m \rangle|_{\omega=\epsilon_m^{G_0W_0}}]$. The derivative of the self-energy is evaluated at $\omega = \epsilon_m$ and $\omega = \epsilon_m^{G_0W_0}$ in Z_m^{linear} and Z_m^{GW100} , respectively. Z_m^{GW100} represents the QP weight (i.e. the pole residue of the Green's function), which equals the area under the Lorentzian QP peak and depends on the spectral weight transfer from the QP peak to satellites and the background.

The second method is to graphically solve the non-linear QP equation in Eq. (6) using the secant (quasi-Newton) method. In this work, we refer to $\epsilon_m^{G_0W_0}$ obtained from the graphical solution as $\epsilon_m^{G_0W_0, \text{graph}}$. The above linearization method corresponds to the first step of the secant method.

The last method is to use the position of the QP peak with the highest spectral weight in the spectral function A_{mm} in Eq. (7). In this work, we refer to $\epsilon_m^{G_0W_0}$ obtained from the spectral function as $\epsilon_m^{G_0W_0, \text{spect}}$ and define Z_m^{spect} by replacing Z_m^{linear} and $\epsilon_m^{G_0W_0, \text{linear}}$ in Eq. (28) by Z_m^{spect} and $\epsilon_m^{G_0W_0, \text{spect}}$, respectively. Note that we searched for the QP peak at $0 < Z_m^{\text{spect}} < 1$ using the peak height instead of the spectral weight (i.e. the area under the peak) due to the practical difficulty of determining the peak range.

G. G_nW_0 and G_nW_n Quasiparticle Energy

As introduced in Section I, there are multiple levels of self-consistency in the GW approximation (from the lowest to the highest): G_0W_0 , G_nW_0 , G_nW_n , QSGW, and SCGW. In this work, we used G_nW_0 and G_nW_n for simplicity, efficiency, and stability. G_nW_0 updates only gKS eigenvalues in G^σ [i.e. ϵ_i^σ and ϵ_a^σ in Eq. (24)], whereas G_nW_n updates gKS eigenvalues in G^σ and \mathbf{A} [i.e. ϵ_i^σ and ϵ_a^σ in Eq. (19)] as well as Casida eigenvalues in W [i.e. Ω_s in Eq. (24)]. Therefore, G_nW_n is computationally more expensive than G_nW_0 by the time to build and diagonalize the RPA Casida-equation matrix in Eq. (18). Note that G_nW_n can be viewed as a diagonal approximation to QSGW.

In this work, we obtained G_nW_0 and G_nW_n QP energies ($\epsilon_m^{G_nW_0}$ and $\epsilon_m^{G_nW_n}$, respectively) by iterating the

recurrence relations ($n \geq 3$):

$$\epsilon_m^{\text{evGW},1} = \epsilon_m + Z^{\text{evGW}} \langle \varphi_m | \Sigma(\epsilon_m) - v_{\text{xc}} | \varphi_m \rangle, \quad (30)$$

$$\begin{aligned} \epsilon_m^{\text{evGW},2} &= \epsilon_m^{\text{evGW},1} \\ &+ Z^{\text{evGW}} \langle \varphi_m | \Sigma(\epsilon_m^{\text{evGW},1}) - \Sigma(\epsilon_m) | \varphi_m \rangle, \quad (31) \\ \epsilon_m^{\text{evGW},n} &= \epsilon_m^{\text{evGW},n-1} \\ &+ Z^{\text{evGW}} \langle \varphi_m | \Sigma(\epsilon_m^{\text{evGW},n-1}) - \Sigma(\epsilon_m^{\text{evGW},n-2}) | \varphi_m \rangle, \quad (32) \end{aligned}$$

where $\epsilon_m^{\text{evGW},n}$ is $\epsilon_m^{G_nW_0}$ or $\epsilon_m^{G_nW_n}$, and $Z^{\text{evGW}} = 1$.

Whereas most GW codes use $0 < Z^{\text{evGW}} < 1$,¹⁶ MOLGW uses $Z^{\text{evGW}} = 1$. In this work, we adopted the choice in MOLGW for a couple of reasons. First, Eq. (32) shows that final converged evGW results are independent of whether $0 < Z^{\text{evGW}} < 1$ or $Z^{\text{evGW}} = 1$. Second, $Z^{\text{evGW}} = 1$ gives a unique and accurate solution, which allows us to avoid the GW multi-solution issue from graphical-solution and spectral-function methods and the ~ 0.1 – 1 eV error from the linearization method (to be discussed later).

There are a few points to note about $Z^{\text{evGW}} = 1$. First, Eqs. (6) and (30) give $\epsilon_m^{G_0W_0} \neq \epsilon_m^{G_1W_0} = \epsilon_m^{G_1W_1}$. In other words, unlike evGW with $0 < Z < 1$, evGW with $Z = 1$ does not use G_0W_0 QP energies. Second, $Z = 1$ in evGW is different from that in QSGW. QSGW interprets that $Z = 1$ accounts for two Z -factor contributions from G and Γ in $\Sigma = iG\Gamma$ (i.e. Z and $1/Z$, respectively).³⁹ However, $Z = 1$ in evGW is not related to the so-called Z -factor cancellation. Last, like QSGW, evGW with $Z = 1$ is a quasiparticle-only (i.e. no-spectral-weight-transfer) GW method, giving no information about plasmon satellites.

One might guess that evGW is computationally more expensive than G_0W_0 by the number of iterations required to reach self-consistency, but this is not the case because the efficiency of evGW depends not only on the number of iterations, but also on other factors. First, without RI, the computational costs for gKS and GW calculations can be comparable [as is the case in this work due to a small prefactor of the AO-MO integral transformation in Eq. (22)], because the 4-center integrals in Eq. (14) are a common bottleneck in both parts. Thus, the cost difference between evGW and G_0W_0 is smaller than the simple guess based on the number of iterations. Second, evGW with $Z^{\text{evGW}} = 1$ needs only one frequency point, whereas G_0W_0 with the linearization method requires two frequency points and the graphical-solution and spectral-function methods require many frequency points. Using only one frequency point has a couple of advantages. One is that it reduces not only the computation time, but also the storage cost. The other is that a test of multiple η and $\Delta\omega$ values is not needed. Last, G_0W_0 needs eigenvalues only for states of interest (e.g. HOMO and/or LUMO), whereas evGW in principle requires eigenvalues for all states. However, in practice, most evGW calculations in the literature update only a few eigenvalues for efficiency without losing much

TABLE I. Number of occupied and empty states for the \uparrow -spin channel ($N_{\text{occ}}^{\uparrow}$ and $N_{\text{emp}}^{\uparrow}$, respectively) used in *GW* calculations. FC means the frozen-core approximation. AE and ECP mean all electron and effective core potential, respectively. CN means the cardinal number.

Anion	Potential	FC	$N_{\text{occ}}^{\uparrow}$	$N_{\text{emp}}^{\uparrow}$			
				CN=2	CN=3	CN=4	CN=5
ScO [−]	AE	Yes	9	67	124	205	314
ScO [−]	AE	No	15	67	124	205	314
TiO [−]	AE	Yes	10	66	123	204	313
TiO [−]	AE	No	16	66	123	204	313
CuO [−]	AE	Yes	13	63	120	201	310
CuO [−]	AE	No	19	63	120	201	310
CuO [−]	ECP	Yes	13	63	120	201	310
CuO [−]	ECP	No	14	63	120	201	310
ZnO [−]	AE	Yes	14	62	119	200	309
ZnO [−]	AE	No	20	62	119	200	309
ZnO [−]	ECP	Yes	14	62	119	200	309
ZnO [−]	ECP	No	15	62	119	200	309

accuracy.^{16,40} For example, when we updated only 21 eigenvalues (for 10 below HOMO, HOMO, and 10 above HOMO) out of ~ 200 while keeping other gKS eigenvalues fixed, we obtained small errors of ~ 100 and ~ 10 meV for 0% and 100% EXX, respectively, in *evGW* IEs of all TMO anions considered in this work. Applying a scissors shift to gKS eigenvalues can make these small errors even smaller. Nevertheless, in this work, we updated all eigenvalues in our *evGW* calculations for accuracy.

III. COMPUTATIONAL DETAILS AND TEST RESULTS

A. Computational Details

Our gKS calculations were carried out using both the MOLGW and the NWChem codes in order to cross-check the results and to ascertain the correct convergence of the SCF cycles. For *GW* calculations, we used the MOLGW code. MOs were expanded using augmented Dunning correlation-consistent Gaussian basis sets, aug-cc-pVnZ ($n = \text{D, T, Q, and 5}$), which are designed to smoothly converge with basis size. Augmentation using diffuse functions is essential in ground-state calculations for anions and in excited-state calculations for both neutrals and anions. Without augmentation, gKS and *GW* eigenvalues for empty states converge very slowly with basis size.^{9,20} In the following, the cardinal number (CN = 2, 3, 4, and 5) is used to represent the approximate size of diverse basis sets employed in the literature and this work. For example, CN = 4 means def2-QZVP in Ref. 12, and aug-cc-pVQZ in this work. Table I summarizes the exact size of CN = 2, 3, 4, 5 basis sets used in this work. To determine the optimized bond lengths of the TMO an-

ions, we used the NWChem code with PBE functional and CN = 3. We obtained bond lengths of 1.695, 1.642, 1.697, and 1.765 Å for ScO⁻, TiO⁻, CuO⁻, and ZnO⁻, respectively.

In order to study the starting-point dependency of the *GW* approximation, we used global hybrid functionals:

$$E_{\text{xc}}^{\text{PBE}\alpha, \sigma} = \alpha E_{\text{x}}^{\text{HF}, \sigma} + (1 - \alpha) E_{\text{x}}^{\text{PBE}, \sigma} + E_{\text{c}}^{\text{PBE}, \sigma}, \quad (33)$$

where $E_{\text{x}}^{\text{HF}, \sigma}$, $E_{\text{x}}^{\text{PBE}, \sigma}$, and $E_{\text{c}}^{\text{PBE}, \sigma}$ are Fock exact exchange, PBE exchange, and PBE correlation energies, respectively. As mentioned earlier in Eq. (12), we refer to the hybrid functionals in Eq. (33) as PBE α functionals in this work. While we tested other functionals such as B3LYP, HSE06, BHLYP, and HF, we discuss only PBE α ($0.00 \leq \alpha \leq 1.00$) results. The main reason for this choice is that the EXX amount in the starting point has a stronger effect on the *GW* results than other factors such as the range separation (to screen the Coulomb interaction) and the correlation type. As shown in the supplementary material, HSE06, PBE0, and BHLYP α (where PBE is replaced by LYP in Eq. 33) at $\alpha=0.25$ give similar *GW* results. Note that the type of the correlation functional is not important (e.g. PBE vs LYP), but the existence of it is. As shown in the supplementary material, PBE α ($\alpha=1.00$) and HF can make a large difference (~ 1 eV) in *GW* results for some states.

B. gKS Test Results

1. Effective Core Potentials

Unlike Sc and Ti, Cu and Zn have two choices of basis sets: AE (All Electron) and ECP (Effective Core Potential). We tested the accuracy and efficiency of ECP with respect to AE to determine whether to use AE for all 3d transition metals or to use AE for Sc and Ti and ECP for Cu and Zn. The test results are presented in the supplementary material. We found that ECP is more efficient than AE not only because the absence of core states makes the basis size smaller, but also because it makes the SCF cycle significantly more stable. However, we also found that there is a spurious difference (~ 0.1 eV) between AE and ECP *GW* results, which increases with the EXX amount. Thus, we conclude that it is not safe to mix AE and ECP for the study of the *GW* starting-point dependency and used only AE for all 3d transition metals in this work.

2. RI for gKS

We did not use RI in this work because our goal is to assess the applicability of the *GW* approximation as accurately as possible using small test molecules, but RI is unavoidable for the practical *GW* study of larger molecules. Thus, we evaluated the quality of RI for both

AE and ECP by comparing RI and no-RI gKS eigenvalues and total spins. The evaluation results are presented in the supplementary material. We found that CN=5 RI ECP causes a large random error in gKS results (e.g. ~ 0.2 and ~ 0.8 eV for CuO^- and ZnO^- , respectively, in gKS-PBE IEs), which decreases with the EXX amount. It is important to note that unlike the SCF convergence error, which occurs only in open-shell systems with non-zero EXX amounts, this gKS RI error occurs in both closed- and open-shell systems with all EXX amounts. It is difficult to detect the gKS RI error because all SCF cycles with different convergence parameters smoothly converge to the same local minimum with no or small spin contamination. Therefore, we conclude that RI should be used only after the potential gKS RI error is thoroughly tested. Note that because we did not use RI (nor ECP) and the 4-center integrals are computed at each SCF step, a *single* gKS calculation is as expensive as a *single* GW calculation in this work, which is consistent with Ref. 9.

3. SCF Convergence Tests

It is not straightforward to obtain the correct mean-field input for GW calculations, because successful convergence of the SCF cycle could come from both correct convergence to the true global minimum as well as wrong convergence to some local minima. This is a particularly critical issue in gKS calculations on open-shell systems involving non-zero EXX and large basis sets. For closed-shell systems or open-shell systems with semi-local xc functionals, the SCF cycle is almost always guaranteed to converge to the global electronic minimum. However, when EXX is used for open-shell systems, wrong convergence occurs frequently and randomly, which makes manual, time-consuming, and error-prone SCF convergence tests mandatory.

In order to obtain the correct mean-field input, we performed three-step SCF convergence tests, as there is no one single indicator of the SCF convergence error that always works. First, we used 12 and 96 sets of SCF convergence parameters for MOLGW and NWChem, respectively, by varying the density mixing scheme in MOLGW, turning on/off molecular symmetry in NWChem, projecting small basis functions to large ones in NWChem, and varying the initial guess wavefunction in both MOLGW and NWChem. Second, we manually searched for correctly converged SCF results using multiple indicators: gKS total energy, total spin $\langle S^2 \rangle$ in Eq. (26), the number of total SCF cycles, a trend over basis size (CN = 2, 3, 4, 5), and a trend over the EXX amount (by manually choosing gKS total energies and total spins that change smoothly with basis size and EXX amount). Last, we cross-checked all MOLGW and NWChem gKS results. Our SCF convergence test results are presented in the supplementary material. Note that because of our heavy SCF convergence tests, *total* gKS

calculations are more expensive than *total* GW calculations in this work.

C. GW Test Results

1. Complete Basis Set Limit

Like MP2, RPA, and CCSD(T) correlation energies, GW QP energies typically converge slowly with the basis size. Accordingly, one should extrapolate GW QP energies obtained from different basis sizes to the complete basis set (CBS) limit to avoid the incomplete basis set error of ~ 0.1 eV.³ We, therefore, tested the effect of the fitting function type, the EXX amount, and the basis size on the GW CBS limit.

Two fitting functions are most widely used for the CBS limit, which we refer to as standard fitting functions in this work:⁴¹

$$E_m = a + \frac{b}{N_{\text{BF}}}, \quad (34)$$

$$E_m = a + \frac{b}{\text{CN}^3}, \quad (35)$$

where E_m are correlation or m th QP energies, a and b are fitting parameters, N_{BF} is the number of basis functions (see Table I), and CN is the cardinal number. In Eqs. (34) and (35), a gives the correlation or QP energy in the CBS limit. Note that there are various non-standard fitting functions used in the literature.^{6,42–45}

Fig. 1 compares CBS results obtained from two standard fitting functions in Eqs. (34) and (35) (as well as one non-standard one used in Refs. 6 and 45). We see that different fitting functions always give different GW CBS limits, deviating from each other by up to ~ 0.1 eV depending on the molecular system and the molecular orbital. Fig. 2 shows the effect of the EXX amount on the GW CBS limit. We observe that the incomplete basis set error increases with the EXX amount. CN = 2 occasionally and randomly causes a significant error (~ 0.1 eV) in the GW CBS limit, which is commonly observed in the literature.^{8,12} Based on these test results, we conclude that it is important to check whether extrapolation is used or not, whether CN = 2 is used or not for extrapolation, and which fitting function is used when analyzing and comparing GW results. For example, Ref. 12 reported that IEs obtained from Gaussian- and planewave-based GW implementations with and without extrapolation, respectively, differ by ~ 0.2 eV, but Refs. 14 and 15 found that the use of PW GW IEs with extrapolation reduces the difference to ~ 0.06 eV. The results reported in this article have been obtained using the fitting function in Eq. (34) with CN = 2, 3, 4, 5.

By enabling MOLGW 1.F to support the largest available basis set (CN = 5), we also tested the effect of CN = 5 on the GW CBS limit. The results are presented in the supplementary material. Here, we briefly mention a couple of trends. In most cases, CN = 5 has

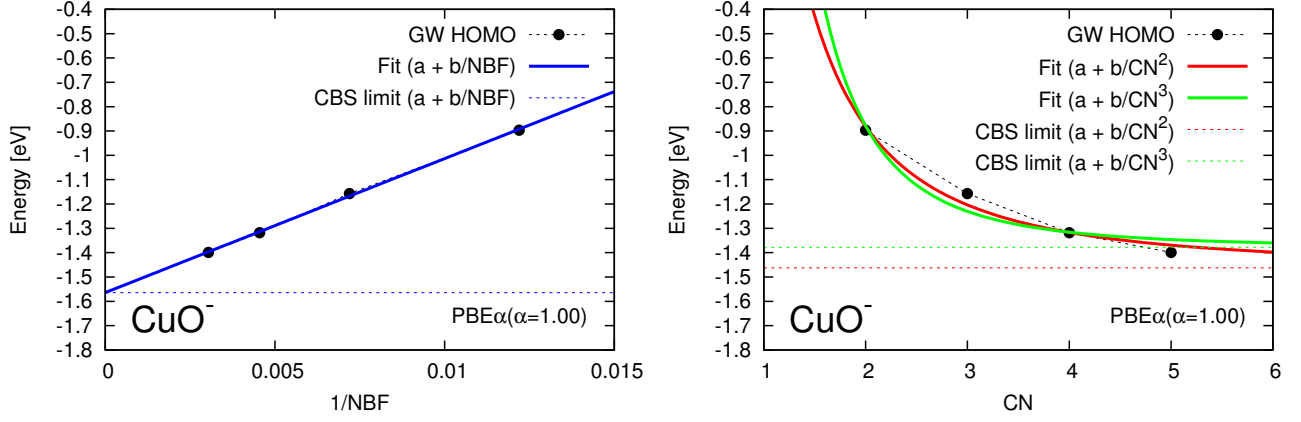


FIG. 1. (Color online) Effect of the fitting function type on the *GW* complete basis set limit. The calculations are presented for the HOMO of CuO^- at the $G_0W_0@PBE\alpha(\alpha = 1.00)$ level of theory. NBF and CN represent the number of basis functions and the cardinal number, respectively.

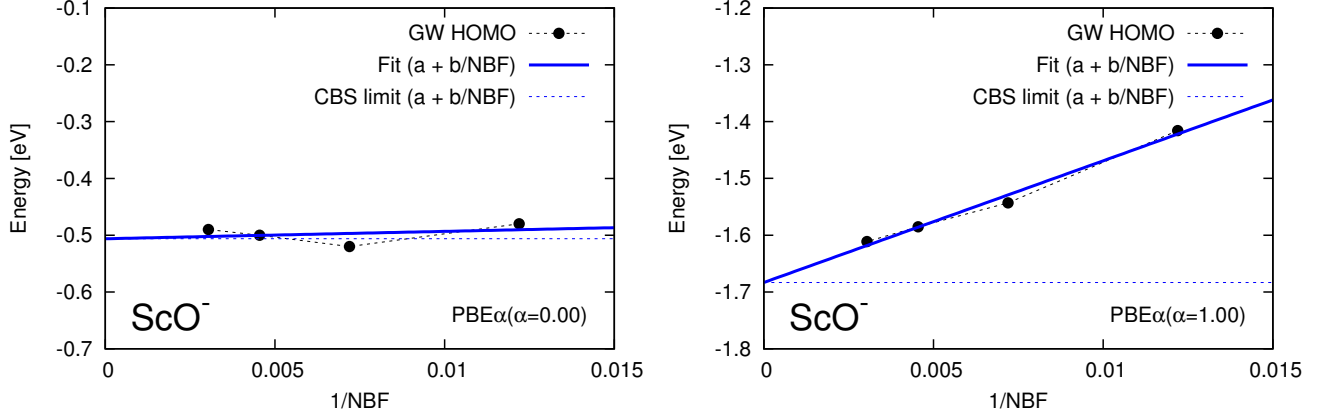


FIG. 2. (Color online) Effect of the EXX amount on the *GW* complete basis set limit. The calculations are presented for the HOMO of ScO^- at the $G_0W_0@PBE$ (left) and $G_0W_0@PBE\alpha(\alpha = 1.00)$ (right) levels of theory. NBF represents the number of basis functions.

a small (~ 10 meV) effect on the *GW* CBS limit, since $\text{CN} = 4, 5$ *GW* QP energies are very similar. However, in some cases, $\text{CN} = 5$ has an appreciable (~ 0.1 eV) effect on the *GW* CBS limit by reducing the effect of the large random $\text{CN} = 2$ error on the *GW* CBS limit. In other words, $\text{CN} = 5$ barely improves the accuracy of the *GW* CBS limit, but mostly acts as a bumper for the $\text{CN} = 2$ error. Moreover, $\text{CN} = 5$ calculations are expensive due to the large number of empty states and the slow SCF convergence speed, and also error-prone due to the high chance of SCF convergence and gKS RI errors. Therefore, we conclude that it is more beneficial to obtain the *GW* CBS limit from $\text{CN} = 3, 4$ than from $\text{CN} = 2, 3, 4, 5$. Using $\text{CN} = 4$ (~ 100 empty states per atom, as shown in Table I) instead of $\text{CN} = 5$ as the largest basis set for the *GW* CBS limit tremendously reduces the computational costs. Note that our conclusion is consistent with Ref. 12, which used only $\text{CN} = 3, 4$ for extrapolation.

Note that the above conclusion holds only for the *GW*

CBS limit for occupied states. We did not test the effect of $\text{CN} = 5$ on the *GW* CBS limit for empty states. As shown in the supplementary material, gKS eigenvalues for empty states are not converged even at $\text{CN} = 5$, which strongly suggests that the *GW* CBS limit for empty states obtained from $\text{CN} = 2, 3, 4, 5$ might be not converged, either. This may be related to the different performances of *GW* for occupied versus empty states discussed in the literature, namely that *GW* tends to give less accurate results for the EA than the IE.^{12,14,15,20,46}

We also tested the effect of the RI approximation on the *GW* CBS limit, which might be useful information for those who want to reproduce the *GW* results reported in this work at lower computational costs without losing too much accuracy. The test results are presented in the supplementary material. We found that RI causes a small consistent error (~ 10 meV) in the *GW* CBS limit, and thus conclude that RI should be used in *GW* calculations whenever possible.

2. Number of Occupied States

We tested the effect of the number of occupied states on GW results using the frozen-core (FC) approximation, which reduces the number of occupied states used in the construction of G and W (see Table I) and thus speeds up GW calculations.⁴ We found that FC approximation causes a very small error (~ 1 – 10 meV) in GW results across all molecular systems, molecular orbitals, and EXX amounts considered in this work. Therefore, we conclude that (except for core-level excitations³³) FC approximation should be used whenever possible, which is consistent with the conclusion in Ref. 4. We note that the use of the FC approximation is recommended not only for efficiency, but also for consistency in the sense that it allows for a fair comparison between AE, ECP, and pseudopotential GW results. We obtained GW results both with and without the FC approximation, but in this work, we present only GW results with FC to help readers reproduce our GW results at lower computational costs using any kind of basis and potential.

3. G_0W_0 Quasiparticle Energy

If we either studied only the IE (and the EA) or used a PPA G_0W_0 method, we could use a single value of η (e.g. 0.1 eV) and a single QP equation solver (e.g. the linearization method). However, we have studied the electronic structure using a full-frequency G_0W_0 method in this work. As such, it is not straightforward to automatically obtain correct and accurate $\epsilon_m^{G_0W_0}$ by using a single value of η and a single QP equation solver due to complicated self-energy pole (and spectral-function peak) structures. Thus, we used three values of η (0.001, 0.002, and 0.005 Ha with $\Delta\omega = 0.001$ Ha) and three QP equation solvers mentioned in Section II F (linearization, graphical-solution, and spectral-function methods).

In a total of nine results for $\epsilon_m^{G_0W_0}$, we observed that $\epsilon_m^{G_0W_0, \text{graph}}$ and $\epsilon_m^{G_0W_0, \text{spect}}$ values are generally identical, whereas $\epsilon_m^{G_0W_0, \text{linear}}$ values are generally different from them by ~ 0.1 – 1 eV. We automatically obtained correct and accurate $\epsilon_m^{G_0W_0}$ from the graphical-solution or spectral-function method using $\eta = 0.002$ or 0.005 Ha when $\epsilon_m^{G_0W_0, \text{graph}}$ and $\epsilon_m^{G_0W_0, \text{spect}}$ were identical. When they were found to be different, we analyzed the results to choose the correct QP energy.

A large distance between ϵ_m and $\epsilon_m^{G_0W_0}$ and multiple self-energy poles between them are responsible for the difficulty of obtaining correct and accurate $\epsilon_m^{G_0W_0}$ for non-frontier orbitals, which is especially the case for local and semi-local xc functionals. Fig. 3 shows various examples of successes and failures of three QP equation solvers for G_0W_0 @PBE QP energies. In the following, we analyze each example individually. Note that we used $\eta = 0.0001$, 0.0002 , and 0.0005 Ha with $\Delta\omega = 0.0001$ Ha in a few of the following examples to demonstrate the danger of small η values for the spectral-function method.

Such small η values are not recommended, as they significantly increase the storage cost while barely improving accuracy.

First, the top two left panels of Fig. 3 show a general example, in which all three methods succeed. We see a few general trends. Typically, all three methods give correct results at $m = \text{HOMO}$ and LUMO , which have a simple pole structure in $\Sigma_c(\omega)$. Graphical-solution and spectral-function methods always give *multiple* solutions, whereas the linearization method gives a *unique* solution, at which two straight lines intersect. Generally, graphical-solution and spectral-function methods give identical (correct and accurate) solutions (in this case, at $\omega = -0.48$ eV), whereas the linearization method gives a different (correct but inaccurate) solution (in this case, at $\omega = -0.69$ eV) due to an intrinsic error of ~ 0.1 – 1 eV. A very small η (0.0002 Ha) sharpens a weak self-energy pole at $\omega = -1.0$ eV in $\Sigma_c(\omega)$, but the sharpened pole *does not* cause an error in the graphical-solution method because it is not between $\epsilon_m^{G_0W_0}$ and ϵ_m . The very small η heightens the weak peak C in $A(\omega)$, but the heightened peak does not cause an error in the spectral-function method because it is still lower than other peaks A and B. In other words, *the spectral-function method depends more weakly on the choice of η than the graphical-solution method*. The very small η has little effect on the linearization method, because (i) the linearization method in this work depends only on $\Sigma_c(\epsilon_m \pm \Delta\omega)$, and (ii) $\omega = -1.0$ eV is too distant from ϵ_m to affect the finite difference method.

Second, the top two right panels of Fig. 3 show a special example, in which the graphical-solution method can give incorrect results. We see a few special trends. Generally, some of the three methods give incorrect results at $m = \text{HOMO}-n$ and $\text{LUMO}+n$ ($n = 1, 2, 3, \dots$), which have a complicated pole structure in $\Sigma_c(\omega)$. A very small η (0.0002 Ha) sharpens a weak pole at $\omega = -2.8$ eV in $\Sigma_c(\omega)$, and this sharpened pole causes a large error of 0.4 eV in the graphical-solution method because it is between $\epsilon_m^{G_0W_0}$ and ϵ_m . The very small η heightens a weak peak B in $A(\omega)$, but the heightened peak does not cause an error in the spectral-function method because it is still lower than the other peak A. The very small η has little effect on the linearization method, because $\omega = -2.8$ eV is distant from ϵ_m .

Third, the bottom two left panels of Fig. 3 show a special example, in which the linearization method can give incorrect results. We see a few special trends. A very small η (0.0002 Ha) sharpens a weak pole at $\omega \approx \epsilon_m$ in $\Sigma_c(\omega)$, but the sharpened pole *does not* cause an error in the graphical-solution method even though it is between $\epsilon_m^{G_0W_0}$ and ϵ_m , because the pole is not sharpened enough ($\eta = 0.0001$ Ha, on the other hand, causes a large error of 1.3 eV). The very small η heightens a weak peak at $\omega \approx \epsilon_m$ in $A(\omega)$, but the heightened peak *cannot* cause an error in the spectral-function method because it is still lower than the other peak at $\omega \approx \epsilon_m^{G_0W_0}$. The very small η sharpens a weak pole at $\omega \approx \epsilon_m$ in $\Sigma_c(\omega)$, and

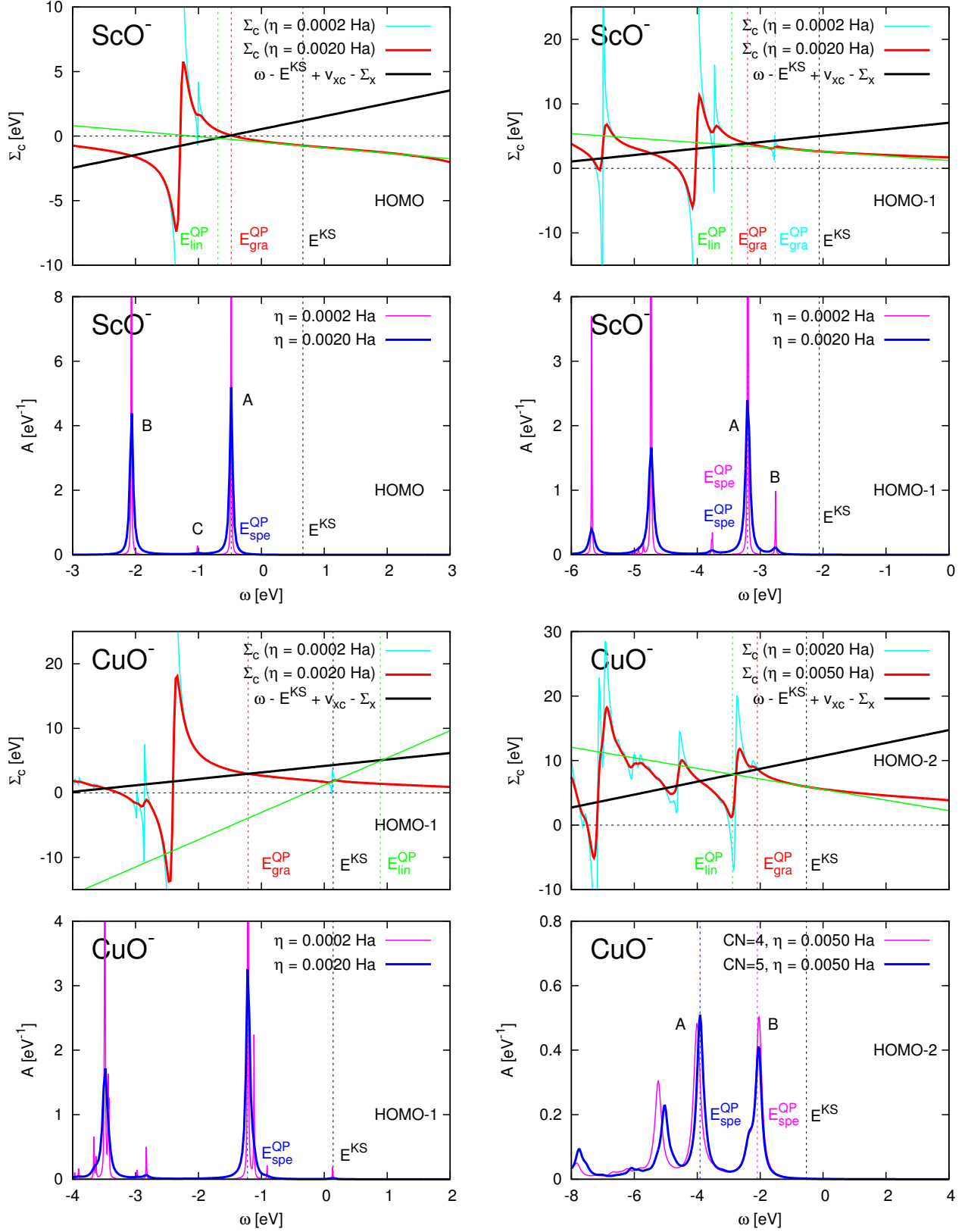


FIG. 3. (Color online) Comparison of three QP equation solvers: linearization, graphical-solution, and spectral-function methods. (Top left) All the three methods give correct results. (Top right) The graphical-solution method can give incorrect results. (Bottom left) The linearization method can give incorrect results. (Bottom right) The spectral-function method can give incorrect results. E^{KS} represents the gKS-PBE eigenvalue. $E_{\text{lin}}^{\text{QP}}$, $E_{\text{gra}}^{\text{QP}}$, and $E_{\text{spe}}^{\text{QP}}$ represent G_0W_0 @PBE QP energies obtained from linearization, graphical-solution, and spectral-function methods, respectively. The green straight line is a tangent to the red curve at $\omega = E^{\text{KS}}$. Except for $A(\omega)$ at the bottom right, all results are obtained from CN=2 no-RI AE.

the sharpened pole makes a large error of 2.1 eV in the linearization method because it is too close to ϵ_m , which makes the finite difference method fail by causing a large error in the slope of the tangent line at $\omega = \epsilon_m$.

Last, the bottom two right panels of Fig. 3 show a special example, in which the spectral-function method can give incorrect results. We see a few special trends. A very small η (0.0002 Ha) sharpens a weak pole at $\omega = -2.3$ eV in $\Sigma_c(\omega)$, but the sharpened pole *does not* cause an error in the graphical-solution method because it is not between $\epsilon_m^{G_0W_0}$ and ϵ_m . Two peaks A and B (at $\omega = -3.9$ and -2.1 eV, respectively) in $A(\omega)$ have similar spectral weights (and peak heights), so it is not straightforward to unambiguously determine which one is a QP peak or a satellite. Spectral weights (practically, peak heights) of the two peaks depend on the basis size: the peak B (A) is higher than the peak A (B) for CN = 2, 3, 4 (CN=5). We chose peak B as the QP peak, because (i) it is consistent with the solution from the graphical-solution method, and (ii) it is consistent with the trend over EXX amount [i.e. G_0W_0 QP energies using the solution from the peak B change smoothly with the EXX amount]. The choice of η and CN has little effect on the linearization method, but $\epsilon_m^{G_0W_0, \text{linear}} = -2.9$ eV causes a large overestimation error of 0.8 eV in the G_0W_0 @PBE binding energy.

There are several points to note about the above examples: (i) we chose simple examples, in which only one method can give incorrect results, for demonstration purposes; multiple methods can give incorrect results simultaneously, as shown in the supplementary material, (ii) not only a very small η (e.g. 0.0002 Ha), but also a very large η (e.g. ~ 0.05 Ha) can cause a large error, as shown in Ref. 47, (iii) deep states (e.g. HOMO- n , where $n = 5, 6, \dots$) have much more complicated pole [peak] structures in $\Sigma_c(\omega)$ [$A(\omega)$] than those in Fig. 3, so it is very difficult to choose correct and accurate $\epsilon_m^{G_0W_0}$ for deep states both automatically and manually.

We conclude this section by summarizing a few guidelines to obtain a reliable and reproducible G_0W_0 @PBE QP spectrum. First, one should try multiple η (and $\Delta\omega$) values. There is no single general η value that works well for all QP equation solvers, molecular systems, and molecular orbitals. In other words, while η is typically viewed as a convergence parameter (i.e. the smaller η , the more accurate GW QP energy), for G_0W_0 and QSGW, it is practically an adjustable parameter, which should be not too small or too large. For example, the optimal value of η depends on $|\epsilon_m^{G_0W_0} - \epsilon_m|$, which is related to the amount of EXX used and how deep the m th state is. Generally, $\sim 10\%$ of $|\epsilon_m^{G_0W_0} - \epsilon_m|$ is a good starting point for the test of η . For example, when calculating G_0W_0 @PBE HOMO and LOMO (lowest occupied molecular orbital) energies, one may try ~ 0.1 and ~ 1 eV, respectively, for η .

Second, we recommend multiple QP equation solvers. As shown in Fig. 3, the G_0W_0 @PBE QP spectrum automatically obtained from a single QP equation solver

can contain a large (~ 1 eV) error at random states. One should manually choose a correct and accurate solution when multiple QP equation solvers give different solutions.

Third, we recommend using multiple basis sizes. As shown in the bottom right of Fig. 3, multiple basis sets with different sizes can give very different G_0W_0 QP energies (by ~ 1 eV) at random states. When it occurs, one should manually choose a correct G_0W_0 QP energy by using a trend over basis size. Using multiple basis sizes allows for not only accurate GW results without small (~ 0.1 eV) systematic errors from the basis set incompleteness, but also correct gKS and GW results without large (~ 1 eV) random errors from SCF convergence and GW multi-solution issues, respectively.

Last, one should be fully aware of the large random errors that can occur with the linearization method, which is the most widely used QP equation solver. Ref. 14 suggests linearization as a preferable method for fairly comparing G_0W_0 @PBE results for the IE (and the EA) from different GW implementations, because it gives a unique solution and thus is free of the GW multi-solution issue. The idea works well for the IE, but it does not perform as well for the QP spectrum. For HOMO (and LUMO), the linearization method generally succeeds and systemically overestimates the IE only by ~ 0.1 eV with respect to the accurate one from the graphical-solution and spectral-function methods, as shown in the top left of Fig. 3, accidentally reducing the ~ 0.5 eV underestimation error by G_0W_0 @PBE with respect to experiment.^{12,14,15} However, for deep states, it randomly succeeds or fails, as shown in the bottom left of Fig. 3, and randomly overestimates or underestimates G_0W_0 @PBE binding energies by ~ 1 eV compared to accurate ones, as shown in the bottom right of Fig. 3 and the supplementary material, respectively. This large and unpredictable (with respect to state, magnitude, and direction) error makes the linearization method inadequate for the G_0W_0 @PBE QP spectrum.

4. G_nW_0 and G_nW_n Quasiparticle Energy

The convergence behaviors of our evGW are shown in the supplementary material. QSGW and our evGW are quasiparticle-only GW methods with no spectral weight transfer (i.e. $Z = 1$), and G_nW_n is a diagonal approximation to QSGW. Therefore, we compared the convergence behaviors of QSGW and our evGW and found a couple of similarities and differences between them.

First, the evGW convergence is reached after only a few iterations, which is consistent with the literature.^{16,40,43} Due to the fast (and stable) convergence, a mixing scheme is not used in our evGW. Unlike evGW, QSGW needs ~ 10 – 20 (up to 60) iterations and a mixing scheme to obtain stably converged results.^{21,46,48}

Second, the orbital character affects the starting-point dependency of evGW. For example, we observed that

TABLE II. TM 3d component in molecular orbitals of TMO anions, where TM = Sc, Ti, Cu, and Zn, obtained from NWChem gKS-PBE results with CN=2 no-RI AE. A bold number represents entire TM 3d character.

	ScO ⁻	TiO ⁻		CuO ⁻	ZnO ⁻	
		↑	↓		↑	↓
HOMO	0.08	1.00	0.00	0.37	0.05	0.06
HOMO-1	0.16	0.12	0.17	0.44	0.05	0.00
HOMO-2	0.16	0.22	0.14	1.00	0.07	
HOMO-3		0.17		0.83		
HOMO-4				0.57		

evGW QP energies for HOMO of CuO⁻ depend more strongly on the EXX amount in the GW starting point than those for HOMO of ScO⁻. We attribute this to the different 3d character strength in HOMO of ScO⁻ and CuO⁻ (8% and 37%, respectively, as shown in Table II). In other words, as the 3d character strength of the molecular orbital increases, the starting-point dependency of evGW increases. We also observed that G_nW_n has a weaker (stronger) starting-point dependency for HOMO of ScO⁻ (CuO⁻) than G_nW_0 . Our results for ScO⁻ are consistent with Ref. 40, which studied the starting-point dependency of evGW using water clusters and concluded that as the self-consistency level of evGW increases from G_nW_0 and G_nW_n , the starting-point dependency of evGW decreases. However, our results for CuO⁻ are not consistent with this trend. This is likely because HOMO of CuO⁻ has a strong 3d character, while those of ScO⁻ and water clusters do not. This orbital-character-dependent starting-point dependency of evGW may be related to conflicting results for QSGW in the literature: Ref. 48 showed the starting-point independency of QSGW using a small *sp*-bonded molecule (CH₄), while Ref. 49 showed the strong starting-point dependency of QSGW using a *d* solid (α -Fe₂O₃).

IV. RESULTS AND DISCUSSION

In this section, we compare our GW calculations to anion PES experiments,^{23–26} focusing especially on the first IE, the lowest 3d-electron binding energy, and the orbital order. We present our results from two approaches separately: First, we discuss non-self-consistent GW with different starting-points (namely, G_0W_0 @PBE α calculations as α is varied in steps of 0.25 from 0 to 1), and then, we discuss eigenvalue self-consistent GW (G_nW_0 and G_nW_n) with PBE starting point. We only briefly discuss our GW results for the starting-point-self-consistency hybrid approach because (i) fundamentally, we found that the hybrid approach does not give any better results than the two separate approaches, and (ii) practically, the hybrid approach inherits disadvantages from both approaches.

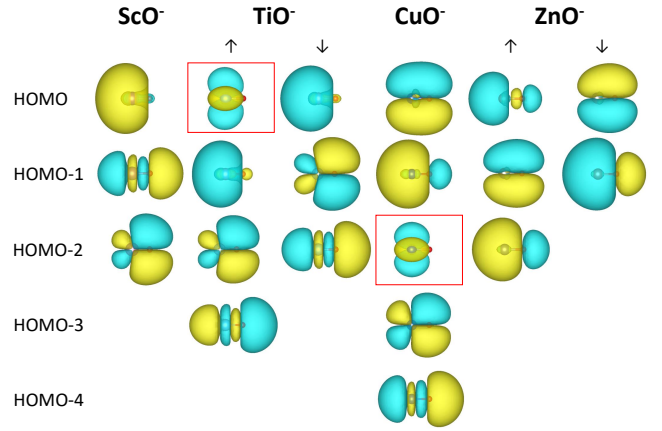


FIG. 4. (Color online) Contour plots of molecular orbitals of TMO anions, where TM = Sc, Ti, Cu, and Zn, from MOLGW gKS-PBE results with CN=2 no-RI AE using VESTA⁵⁰. A red box represents entire TM 3d character.

ScO⁻, TiO⁻, CuO⁻, and ZnO⁻ are similar but different systems in several aspects. First, ScO⁻ and CuO⁻ are closed-shell systems, whereas TiO⁻ and ZnO⁻ are open-shell systems. Second, ScO⁻ and TiO⁻ have partially filled 3d shells, while CuO⁻ and ZnO⁻ have completely filled 3d shells. Third, TiO⁻ has shallow 3d states, but CuO⁻ and ZnO⁻ have deep 3d states. Fourth, 3d-electron photodetachment transitions are observed in TiO⁻ and CuO⁻, but not in ScO⁻ and ZnO⁻. Furthermore, CuO⁻ has strong 3d character in the HOMO, but ScO⁻, TiO⁻, and ZnO⁻ have weak 3d character in the HOMO. Last, two-electron transitions are observed in ScO⁻, but not in TiO⁻, CuO⁻, and ZnO⁻. Due to these similarities and differences, TMO anions are an ideal set of systems for the evaluation of the performance of GW schemes.

Table II shows the amount of TM 3d character in all molecular orbitals considered in this work, obtained from gKS-PBE. We find that \uparrow -HOMO of TiO⁻ and HOMO-2 of CuO⁻ have entirely TM 3d character. Fig. 4 shows the contour plots of all molecular orbitals considered in this work, obtained from gKS-PBE. It is clearly seen that \uparrow -HOMO of TiO⁻ and HOMO-2 of CuO⁻ are strongly localized on Ti and Cu, respectively. Note that when analyzing GW calculations, we used only the gKS-PBE orbital order to avoid confusion. It is well known that the orbital ordering observed with PBE can change as a function of the amount of EXX and after a GW calculation^{8,15}. In this work, gKS-PBE and G_0W_0 @PBE were found to have the same orbital order. Table III summarizes all of our GW calculations with comparison to PES experiments and existing calculations in the literature.

TABLE III. Experimental and calculated electron binding energies of TMO anions (in eV). MAE represents the mean absolute error. Bold numbers represent $3d$ -electron binding energies.

		$G_0W_0@PBE\alpha$					$G_nW_0@$	$G_nW_n@$		
	State	Exp.	$\alpha=0.00$	$\alpha=0.25$	$\alpha=0.50$	$\alpha=0.75$	$\alpha=1.00$	PBE	PBE	Others
ScO ⁻ (¹ Σ^+)										
HOMO	¹ Σ^+	1.35 ^a	0.51	1.15	1.45	1.59	1.63	1.21	1.35	1.28 ^g , 1.26 ^j , 1.19 ^k
HOMO-1	² Δ	3.10 ^a	3.30	4.77	5.45	5.72	5.82	5.34	6.08	2.41 ^g , 2.78 ^h , 3.31 ⁱ
HOMO-2	² Π	3.40 ^a	3.42	4.81	5.40	5.61	5.63	5.39	6.17	3.34 ^g , 3.24 ^h , 3.44 ⁱ
MAE			0.84 ^e	0.18 ^e	0.10 ^e	0.24 ^e	0.28 ^e	0.14 ^e	0.00 ^e	
TiO ⁻ (² Δ)										
\uparrow -HOMO	¹ Σ^+	2.00^b	0.26	2.24	3.70	4.79	5.63	1.83	2.74	2.39 ^g , 2.37 ^h , 2.34 ⁱ
\uparrow -HOMO-1	¹ Δ	1.73 ^b	0.53	1.28	1.65	1.83	1.95	1.38	1.61	1.88 ^g , 1.72 ⁱ
\downarrow -HOMO	³ Δ	1.30 ^b	0.31	1.00	1.29	1.43	1.55	1.06	1.21	1.19 ^g , 1.18 ^j , 1.14 ⁿ
MAE			1.31	0.33	0.60	1.01	1.37	0.25	0.32	
CuO ⁻ (¹ Σ^+)										
HOMO	² Π	1.78 ^c	0.40	1.40	1.58	1.40	0.97	2.19	3.17	1.55 ^g , 1.52 ^j , 0.46 ^o
HOMO-1	² Σ^+	2.75 ^c	1.39	2.17	2.23	1.98	1.56	2.66	3.58	2.96 ^g , 2.86 ^h , 1.60 ^o , 2.78 ^p , 2.47 ^q , 2.81 ^r , 2.54 ^s
HOMO-2		4.50^f	2.18	4.05	4.60	4.56	4.25	4.88	6.38	4.07 ^g , 4.01 ^h , 4.58 ^p , 4.50 ^q
HOMO-3			2.89	4.49	5.06	5.04	4.67	4.96	6.60	
HOMO-4			3.70	4.49	4.63	4.53	4.24	5.16	6.39	
MAE			1.69	0.47	0.27	0.40	0.75	0.29	1.37	
ZnO ⁻ (² Σ^+)										
\uparrow -HOMO	¹ Σ^+	2.09 ^d	0.91	1.91	2.20	2.23	2.00	2.11	2.57	2.19 ^g , 2.33 ^j , 2.29 ^l , 2.10 ^m , 1.06 ^o
\uparrow -HOMO-1	¹ Π	2.71 ^d	1.36	2.43	3.03	3.72	4.79	2.77	3.73	2.62 ^g , 1.43 ^o
\uparrow -HOMO-2			3.24	4.04	4.89	5.64	6.90	4.77	5.66	3.50 ^o
\downarrow -HOMO	³ Π	2.40 ^d	1.17	2.17	2.64	3.15	4.02	2.65	3.48	2.41 ^g , 1.20 ^o
\downarrow -HOMO-1	³ Σ^+	3.96 ^d	2.71	3.35	3.47	3.31	3.00	4.11	4.51	4.15 ^g , 2.89 ^o
MAE			1.25	0.33	0.29	0.64	1.19	0.12	0.78	

^a Ref. 23

^b Ref. 24

^c Ref. 25

^d Ref. 26

^e HOMO-1 and HOMO-2 are not included because our GW calculations cannot account for two-electron transitions (see text).

^f We chose this value from the Z band in the PES spectrum of CuO⁻ (see text).

^g Ref. 51 using 6-3111+G* basis sets

^h Ref. 52

ⁱ Ref. 53 using the multi-reference configuration interaction (MRCI) method

^j Ref. 10 using the B3LYP functional

^k Ref. 11 using the B3LYP functional

^l Ref. 54 using the B3LYP functional

^m Ref. 20 using the $G_0W_0@PBE0$ method

ⁿ Ref. 55 using the B3LYP functional

^o Ref. 47 using the $G_0W_0@PBE$ method

^p Ref. 56 using the CCSD(T) method

^q Ref. 57

^r Ref. 58 using the single and double excitation configuration interaction (SDCI) method

^s Ref. 59

A. G_0W_0 Starting Points

Figs. 5 and 6 show PES and $G_0W_0@PBE\alpha(0.00 \leq \alpha \leq 1.00)$ QP spectra of ScO⁻, TiO⁻, CuO⁻, and ZnO⁻. In PES spectra, vertical dashed and solid lines represent experimental sp - and d -electron binding energies, respectively. In GW spectra, oblique dashed and solid lines track calculated sp - and d -electron binding energies, re-

spectively. In Figs. 5 and 6, we find a few general trends common in all TMO anions considered in this work: (i) no $G_0W_0@PBE\alpha(0.00 \leq \alpha \leq 1.00)$ results are in perfect agreement with experiment, (ii) $G_0W_0@PBE$ underestimates the IE of TMO anions by ~ 1 eV, which is larger than the typical underestimation for sp molecules (~ 0.5 eV),^{12,14,15} and (iii) $G_0W_0@PBE\alpha(0.25 \leq \alpha \leq 0.50)$ reduces it to ~ 0.1 eV. In the following, we analyze

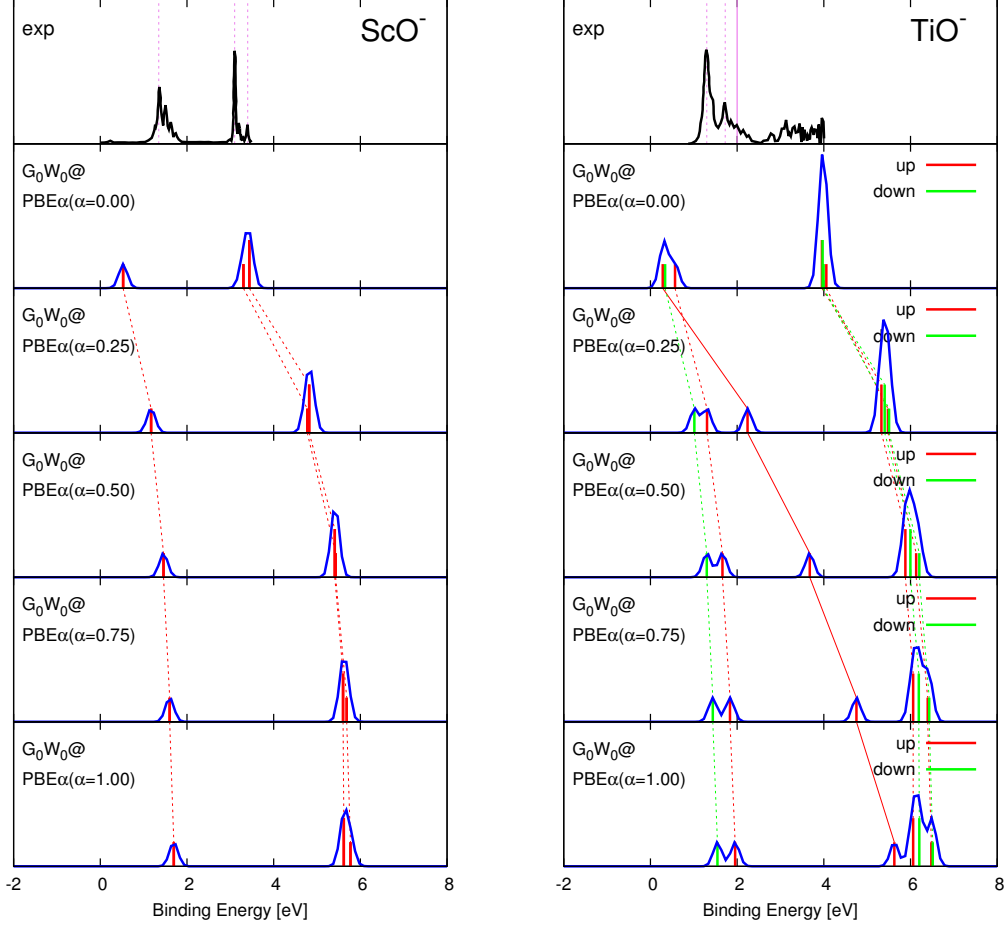


FIG. 5. (Color online) Effect of the EXX amount in the G_0W_0 starting point on the electronic structure of ScO^- and TiO^- . A Gaussian distribution function with a smearing width of 0.1 eV is used to broaden the spectra.

each TMO anion individually.

1. ScO^-

Scandium is the first transition metal and has only one 3d electron. DFT and CCSD(T) calculations in Refs. 10 and 11 confirmed the ground state of ScO^- as $^1\Sigma^+$ ($8\sigma^2 3\pi^4 9\sigma^2$), correcting the wrongly assumed state $^3\Delta^-$ ($8\sigma^2 3\pi^4 9\sigma^1 1\delta$) in Ref. 23. There is no 3d peak or band in the PES spectrum of ScO^- , and the top three valence molecular orbitals have weak Sc 3d character (8%, 16%, and 16%, respectively), as shown in Table II.

In the left panel of Fig. 5, we see that for HOMO-1 and HOMO-2 of ScO^- , G_0W_0 @PBE binding energies slightly overestimate PES ones (by 0.20 and 0.02 eV for HOMO-1 and HOMO-2, respectively), whereas G_0W_0 @PBE α ($0.25 \leq \alpha \leq 1.00$) binding energies significantly overestimate PES ones by ~ 2 eV (e.g. for HOMO-1, G_0W_0 @PBE α ($\alpha=0.25$) and G_0W_0 @PBE α ($\alpha=1.00$)).

binding energies are greater than PES ones by 1.67 and 2.72 eV, respectively). This seems to suggest that for HOMO-1 and HOMO-2 of ScO^- , G_0W_0 @PBE performs better than G_0W_0 @PBE α ($0.25 \leq \alpha \leq 1.00$), but this is not the case, due to the nature of the corresponding peaks in the PES experiment. Ref. 11 suggests that the second and third peaks in the PES spectrum of ScO^- are likely due to two-electron transitions from $8\sigma^2 3\pi^4 9\sigma^2$ ($^1\Sigma^+$ ScO^-) to $8\sigma^2 3\pi^4 10\sigma$ ($B^2\Sigma^+$ ScO) and to $8\sigma^2 3\pi^4 1\delta$ ($A'^2\Delta$ ScO) states, respectively, which GW calculations for quasiparticle excitations cannot account for. In other words, the seemingly excellent agreement between G_0W_0 @PBE and PES binding energies for HOMO-1 and HOMO-2 of ScO^- is accidental. Therefore, we exclude HOMO-1 and HOMO-2 of ScO^- from our evaluation of the performance of GW schemes in the following.

We also see that as α increases, the G_0W_0 @PBE α IE always increases, but this happens at different rates: As α increases from 0.00 to 0.25, it increases rapidly, whereas

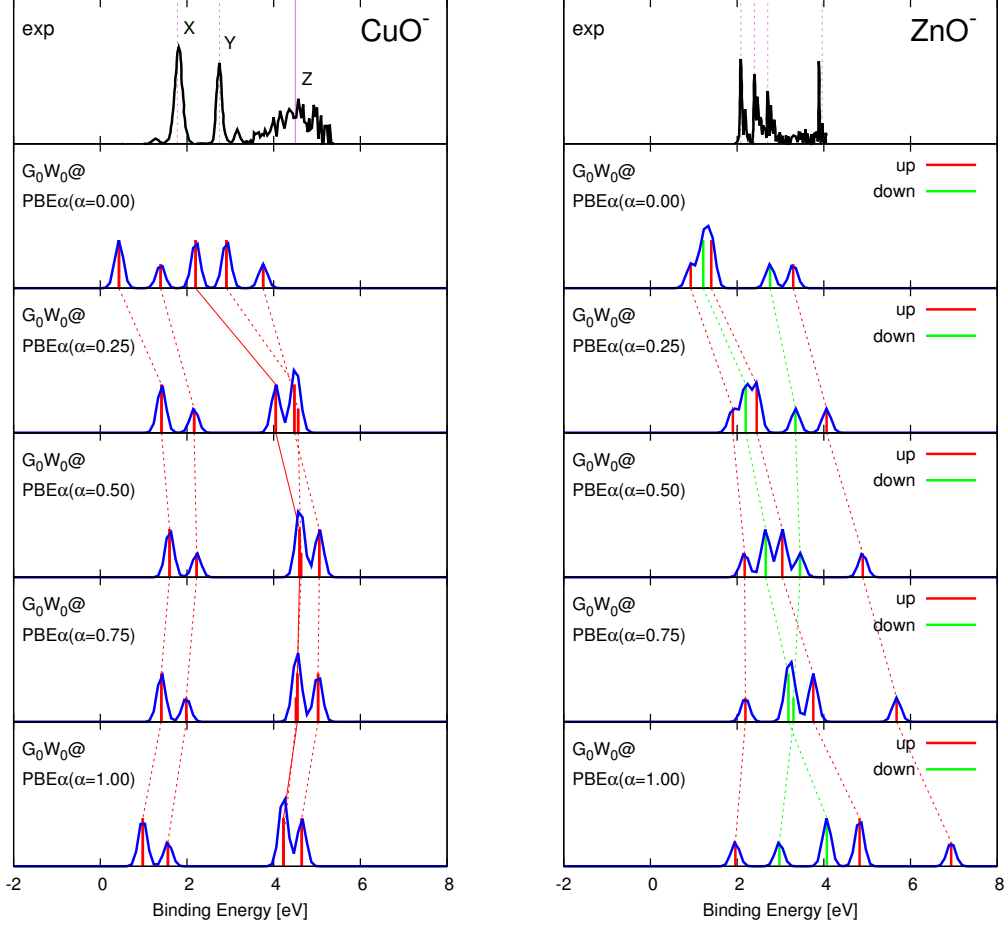


FIG. 6. (Color online) Effect of the EXX amount in the G_0W_0 starting point on the electronic structure of CuO^- and ZnO^- . A Gaussian distribution function with a smearing width of 0.1 eV is used to broaden the spectra.

as α increases from 0.25 to 1.00, it increases slowly. The weak sensitivity of the $G_0W_0@PBE\alpha(\alpha \geq 0.25)$ IE to a change in α gives a large margin for an optimal amount of EXX: 25%–100%.

2. TiO^-

Titanium is the second transition metal and has two 3d electrons. Several theoretical studies in Refs. 10, 51, 53, 55, and 60 confirmed $9\sigma^2\delta^1$ ($^2\Delta$) as the ground-state electron configuration of TiO^- , correcting the wrongly assigned configuration $9\sigma^1\delta^2$ ($^1\Sigma^+$) in Ref. 24. Unlike ScO^- , which has an empty δ shell, TiO^- has one 3d electron in the δ shell. The transition of the 3d electron from $9\sigma^2\delta^1$ ($^2\Delta$ TiO^-) to $9\sigma^2$ ($^1\Sigma^+$ TiO) states produces the third peak in the PES spectrum of TiO^- at 2.0 eV. In the $G_0W_0@PBE\alpha$ QP spectrum of TiO^- , \uparrow -HOMO is of entirely Ti 3d character, as shown in Table II.

The right panel of Fig. 5 clearly shows that the

$G_0W_0@PBE\alpha(0.00 \leq \alpha \leq 1.00)$ QP energy for \uparrow -HOMO of TiO^- is much more sensitive to a change in α than those for other occupied molecular orbitals with mainly *sp* character, as shown in Table II. The orbital-character-dependent sensitivity of the $G_0W_0@PBE\alpha$ QP energy to a change in α causes a couple of problems. First, $G_0W_0@PBE$ underestimates the IE and the 3d-electron binding energy of TiO^- non-uniformly (by 0.99 and 1.74 eV, respectively), leading to the wrong orbital order. In other words, G_0W_0 does not correct the wrong orbital order produced by PBE. Second, the G_0W_0 starting-point approach does not give accurate results for both the IE and the 3d-electron binding energy of TiO^- at the same time. For example, $G_0W_0@PBE\alpha(\alpha=0.50)$ gives a better result for the IE of TiO^- by 0.29 eV, but a worse result for the 3d-electron binding energy of TiO^- by 1.46 eV, than $G_0W_0@PBE\alpha(\alpha=0.25)$. This type of behavior is not uncommon in *GW* predictions for transition metal oxides; for example, no existing *GW* scheme can accurately reproduce both the bandgap and the *d*-

band position in the band structure of bulk ZnO at the same time.^{16–18}

The increase in α from 0 to 1 has a similar effect on the $G_0W_0@PBE\alpha$ IE of both ScO^- and TiO^- : For both ScO^- and TiO^- , $G_0W_0@PBE\alpha$ ($0.25 \leq \alpha \leq 1.00$) reduces the underestimation of the IE by $G_0W_0@PBE$ from ~ 1 eV to ~ 0.1 eV [e.g. $G_0W_0@PBE\alpha$ ($\alpha=0.25$) reduces the difference in the IE between PES and $G_0W_0@PBE$ from 0.84 eV to 0.20 eV and from 0.99 eV to 0.30 eV, respectively]. However, unlike ScO^- , the strong sensitivity of the $G_0W_0@PBE\alpha$ 3d-electron binding energy of TiO^- to a change in α gives a small margin for an optimal amount of EXX, which is $\sim 25\%$.

3. CuO^-

Copper is the 11th transition metal and has ten 3d electrons. DFT calculations in Ref. 10 confirmed the ground state of CuO^- as $^1\Sigma^+$ with the electron configuration of $3d^{10}2p\sigma^22p\pi^4$. There are three bands (named as X, Y, and Z in Ref. 25) in the PES spectrum of CuO^- , as shown in the top of the left panel of Fig. 6. Ref. 25 suggested that the photodetachment transition of 3d electrons ($3d\delta^43d\pi^43d\sigma^2$) from $^1\Sigma^+$ CuO^- $3d^{10}2p\sigma^22p\pi^4$ to Z CuO $3d^92p\sigma^22p\pi^4$ states produces the broad Z band in the PES spectrum of CuO^- at ~ 4.5 eV (which we selected from the position of the highest peak in the Z band) and assumed that the Z band is unusually broad likely due to a large geometry change from the anion to the neutral. In the $G_0W_0@PBE\alpha$ QP spectrum of CuO^- , HOMO-2 is of entirely Cu 3d character, as shown in Table II.

In the left panel of Fig. 6, we see that the $G_0W_0@PBE\alpha$ ($0.00 \leq \alpha \leq 0.50$) QP energy for HOMO-2 of CuO^- is more sensitive to a change in α than those for other occupied molecular orbitals with weaker Cu 3d character than HOMO-2, as shown in Table II, and $G_0W_0@PBE\alpha$ ($\alpha=0.50$) gives good results for the IE and the 3d-electron binding energy (corresponding to HOMO and HOMO-2, respectively) of CuO^- at the same time. This is consistent with the $G_0W_0@BHLYP$ result reported for CuO^- reported in Ref. 45. Like TiO^- , the orbital-character-dependent sensitivity of the $G_0W_0@PBE\alpha$ QP energy to a change in α causes $G_0W_0@PBE$ to underestimate the IE and the 3d-electron binding energy of CuO^- non-uniformly (by 1.38 and 2.32 eV, respectively). $G_0W_0@PBE\alpha$ ($0.50 < \alpha \leq 1.00$) QP energies for all valence molecular orbitals considered in this work are weakly sensitive to a change in α possibly because $PBE\alpha$ ($0.50 < \alpha \leq 1.00$) orbitals with large amounts of EXX are good for localized states of CuO^- with strong 3d character [i.e. for CuO^- , $PBE\alpha$ ($0.50 \leq \alpha \leq 1.00$) wavefunctions are close to QP ones].

4. ZnO^-

Zinc is the 12th transition metal and has ten 3d electrons. Zinc is rather distinct from other first row transition metals due to its closed-shell electron configuration. In other words, zinc is more similar to alkaline earth metals than other transition metals because Zn 3d electrons generally do not participate in bonding.⁶¹ DFT calculations in Ref. 10 confirmed the ground-state electron configuration of ZnO^- as $^2\Sigma^+ 10\sigma^19\sigma^24\pi^4\delta^4$. There are four bands in the PES spectrum of ZnO^- , as shown in the top of the right panel of Fig. 6. Due to the relatively low photon energy of 4.66 eV used in the experiments,²⁶ these four bands are not associated with the photodetachment of 3d electrons. Unlike CuO^- , all valence molecular orbitals in the $G_0W_0@PBE\alpha$ QP spectrum of ZnO^- have weak Zn 3d character, as shown in Table II.

The right panel of Fig. 6 shows that unlike CuO^- , $G_0W_0@PBE$ underestimates electron binding energies for all valence molecular orbitals of ZnO^- uniformly (e.g. by 1.18, 1.35, 1.23, and 1.25 eV for \uparrow -HOMO, \uparrow -HOMO-1, \downarrow -HOMO, and \downarrow -HOMO-1, respectively) possibly because all valence molecular orbitals have similar Zn 3d character and thus their $G_0W_0@PBE\alpha$ QP energies have similar sensitivity to a change in α . Like CuO^- , $G_0W_0@PBE\alpha$ ($\alpha=0.50$) gives good results for the IE and the orbital order of ZnO^- at the same time. Unlike CuO^- , $G_0W_0@PBE\alpha$ ($0.50 < \alpha \leq 1.00$) QP energies for all valence molecular orbitals, except for HOMO and \downarrow -HOMO-1, are strongly sensitive to a change in α . This trend is observed already at the gKS level (before applying the one-shot GW correction), and can be explained in terms of the importance of spin-splitting in open-shell molecules, as has been discussed in Ref. 45 for the case of CuO_2^- molecule.

B. evGW Self-Consistency Levels

Fig. 7 shows PES and evGW QP spectra of ScO^- , TiO^- , CuO^- , and ZnO^- . In the following, we analyze $G_nW_0@PBE$ and $G_nW_n@PBE$ results individually.

In Fig. 7, we see that as the self-consistency level increases from G_0W_0 to G_nW_n , GW binding energies always increase, but this occurs at different rates: As the self-consistency level increases from G_0W_0 to G_nW_0 , GW binding energies increase rapidly (e.g. the IE increases by 0.70, 0.75, 1.79, and 1.20 eV for ScO^- , TiO^- , CuO^- , and ZnO^- , respectively), whereas as the self-consistency level increases from G_nW_0 to G_nW_n , they increase slowly (e.g. the IE increases by 0.14, 0.15, and 0.46 eV for ScO^- , TiO^- , and ZnO^- , respectively), except for CuO^- where the increase is ~ 1 eV, which will be discussed later. $G_0W_0@PBE$ always underestimates electron binding energies, whereas $G_nW_n@PBE$ generally overestimates them. $G_nW_0@PBE$ electron binding energies are always in between $G_0W_0@PBE$ and $G_nW_n@PBE$ ones, and they are generally close to experiment. In other

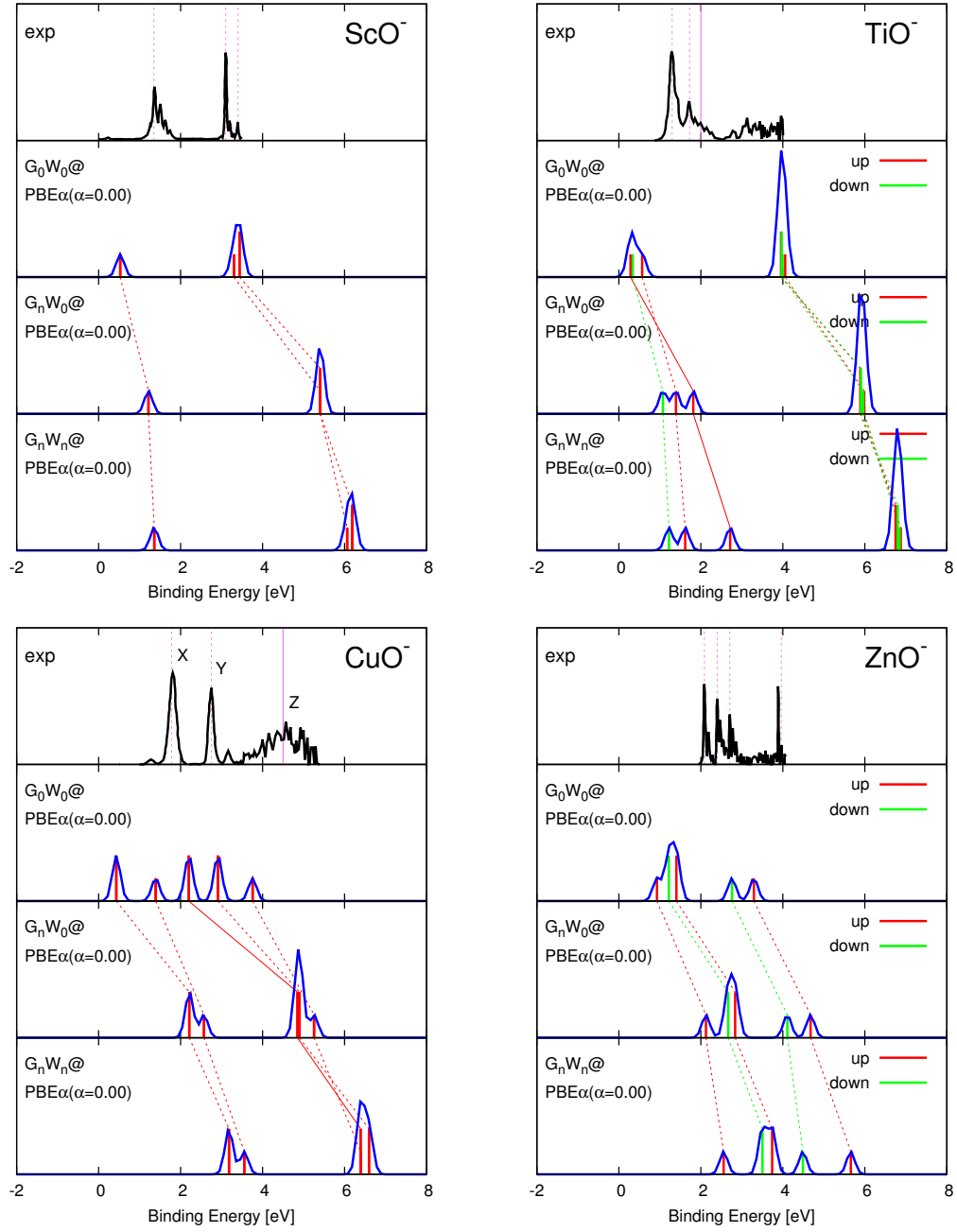


FIG. 7. (Color online) Effect of the $evGW$ self-consistency level on the electronic structure of ScO^- , TiO^- , CuO^- , and ZnO^- . A Gaussian distribution function with a smearing width of 0.1 eV is used to broaden the spectra.

words, $G_0W_0@PBE$ and $G_nW_n@PBE$ act as lower and upper bounds for $G_nW_0@PBE$, generally producing over- and under-screenings, respectively. This trend of the $evGW$ self-consistency approach in the electronic structure of molecules is also observed in the band structure of solids.¹⁶

We also see that the $evGW$ self-consistency has a strong effect on the GW binding energy for molecular orbitals with strong $3d$ character (e.g. \uparrow -HOMO of TiO^- and HOMO-2 of CuO^-). For example, $G_nW_0@PBE$ re-

duces the underestimation errors of $G_0W_0@PBE$ in the IE and the $3d$ -electron binding energies of TiO^- with respect to experiment from 0.99 and 1.74 eV to 0.24 and 0.17 eV, respectively. As a result, $G_nW_0@PBE$ corrects the wrong $G_0W_0@PBE$ orbital order in TiO^- . Another example is that $G_nW_0@PBE$ gives small (~ 0.1 eV) errors in electron binding energies for all valence molecular orbitals of ZnO^- , which are underestimated by $G_0W_0@PBE$ uniformly by ~ 1 eV due to the similarly weak Zn $3d$ character. For ZnO^- , $G_0W_0@PBE$ and

G_nW_0 @PBE result in mean absolute errors (MAEs) of 1.25 and 0.12 eV, respectively, as shown in Table III.

CuO^- exhibits particularly large differences between binding energies computed at the G_nW_0 @PBE and G_nW_n @PBE levels compared to other TMO anions. We attribute this to the stronger $3d$ character of CuO^- molecular orbitals. For example, CuO^- has a larger difference between G_nW_0 @PBE and G_nW_n @PBE IEs than ScO^- (e.g. 0.98 and 0.14 eV, respectively) possibly because HOMO of CuO^- has stronger $3d$ character than that of ScO^- (e.g. 37% and 8%, respectively, as shown in Table II). This is also consistent with the observation that the largest difference between G_nW_0 @PBE and G_nW_n @PBE predictions for the case of TiO^- occurs for the $^1\Sigma^+$ state (0.91 eV shift), which has a pure $3d$ character, compared to $^1\Delta$ and $^3\Delta$ states (0.23 and 0.15 eV shifts), which have weak $3d$ character.

C. Comparison of G_0W_0 starting-point and evGW self-consistency approaches

From our results presented so far, it appears that both G_0W_0 starting-point and evGW self-consistent approaches can, in principle, be good GW methods for finite systems: both G_0W_0 @PBE α ($0.25 \leq \alpha \leq 0.50$) and G_nW_0 @PBE can reduce the large and orbital-character-dependent non-uniform errors for electron binding energies of TMO anions produced by G_0W_0 @PBE with respect to experiment from ~ 1 –2 eV to ~ 0.1 –0.5 eV. Ref. 17 obtained a similar result for extended systems: both G_0W_0 @PBE α ($\alpha=0.25$) and G_nW_0 @PBE give satisfactory results for the bandgap and the d -electron binding energy of solids, and drew the conclusions that (i) for accuracy, one can choose either G_0W_0 @PBE α ($\alpha=0.25$) or G_nW_0 @PBE because they give similar results, but (ii) for efficiency, one may want to choose G_0W_0 @PBE α ($\alpha=0.25$) over G_nW_0 @PBE because the former is computationally cheaper than the latter. However, in the case of molecular systems, we argue that G_nW_0 @PBE has several practical advantages over G_0W_0 @PBE α .

First, G_nW_0 @PBE does not contain system-dependent adjustable parameters. Unlike extended systems, there is no unique amount of EXX for the G_0W_0 starting point, which works well for all finite systems. For example, we showed in Section IV A that 25% EXX is optimal for ScO^- and TiO^- , whereas 50% EXX is optimal for CuO^- and ZnO^- . Also, it appears that atoms and small molecules require more amount of EXX than clusters and large molecules.⁴⁰ Second, G_nW_0 @PBE is transferable between finite and extended systems. G_nW_0 @PBE works well for both molecules and solids (e.g. ZnO^- anion and bulk ZnO , respectively).¹⁶ This greatly extends the applicability of the GW method. For example, G_nW_0 @PBE may be applicable to solid-molecule hybrid systems such as molecular junctions and molecules adsorbed on solid surfaces.⁶² Also, G_nW_0 @PBE may be used for the study

of quantum size effects in clusters because it is independent of the cluster size. Third, G_nW_0 @PBE is transferable between closed- and open-shell systems, as PBE is free of the EXX-induced SCF convergence error (e.g. spin contamination) that frequently and randomly occurs in open-shell systems. Fourth, G_nW_0 @PBE is easy to use and reliable. As explained in detail in Section III, G_0W_0 @PBE α in Gaussian-based GW implementations requires manual, time-consuming, and error-prone tests at each step towards the QP spectrum and does not guarantee to give reliable and reproducible results mainly because of two issues: (i) the SCF convergence issue at gKS calculations, and (ii) the GW multi-solution issue at some QP equation solvers. PBE avoids the EXX-induced SCF convergence error by not using EXX, and evGW can avoid the GW multi-solution issue by using the non-spectral-weight-transfer (quasiparticle-only) approximation.

Furthermore, G_nW_0 @PBE has a few desirable properties. Two of these come from the PBE part. PBE causes the smallest incomplete basis set error, as shown in Fig. 2, allowing one to use smaller basis sets for the CBS limit, which makes G_nW_0 @PBE cheaper. PBE also produces the smallest difference between AE and ECP results (the difference between AE and ECP results increases with the EXX amount) as discussed in Section III B 1, which allows one to fully take advantage of ECP for both light and heavy transition metals. Also, ECP is cheaper and gives faster SCF convergence than AE due to the absence of core states as discussed in Section III B 1. Two desirable properties come from the GW part. G_nW_0 (as well as G_nW_n) gives faster and more stable GW convergence than QSGW, as discussed in Section III C 4, and depends more weakly on the choice of η . Also, G_nW_0 is cheaper than G_nW_n , as pointed out in Ref. 16 and discussed in Section II G. In fact, G_nW_0 is the cheapest self-consistent GW scheme.

One may argue that G_0W_0 @PBE α should be a choice of GW methods because it is computationally more efficient than G_nW_0 @PBE by the number of self-consistent GW iterations. However, as discussed in Section II G, this is not the case since the computation time difference between G_0W_0 @PBE α and G_nW_0 @PBE does not depend only on the number of self-consistent GW iterations; there are other factors such as the number of eigenvalues to update for $\epsilon_m^{G_nW_0}$, the number of frequency points to use for $\Sigma_c(\omega)$, the number of $\Delta\omega$ and η values to test for $\epsilon_m^{G_0W_0}$, and the number of initial guess wavefunctions to test for gKS calculations. Some factors can cancel each other out; for example, G_nW_0 @PBE requires a few self-consistent GW iterations, but one typically needs to test a few η values for G_0W_0 @PBE α . In other words, when all factors are taken into account, the total computation time to obtain reliable and reproducible QP spectra at G_0W_0 @PBE α and G_nW_0 @PBE levels of theory can be comparable, as is especially the case for open-shell systems.

TABLE IV. Optimal amount of EXX in the G_0W_0 starting point for gas-phase small molecules (highlighted in bold).

Reference	Körbel <i>et al.</i> ²⁰	Bruneval <i>et al.</i> ⁴	Kaplan <i>et al.</i> ²¹	Rostgaard <i>et al.</i> ²²	This work
Code	FIESTA	MOLGW	TURBOMOLE	GPAW	MOLGW
Optimal EXX	25%	50%	75%	100%	25–50%
Tested EXX	25 & 100%	0, 20, 25 & 50%	0, 25 & 75%	0 & 100%	0, 25, 50, 75 & 100%
System	39 closed-shell 3,4,5d & 9 closed-shell <i>sp</i>	34 closed-shell <i>sp</i> ^a	29 closed-shell <i>sp</i>	34 closed-shell <i>sp</i> ^a	4 closed- & open-shell 3d
System size	2–7 atoms	2–8 atoms	2–18 atoms	2–8 atoms	2 atoms
Property	HOMO & LUMO	HOMO	HOMO & HOMO- <i>n</i> (<i>n</i> = 0, 1, ...) ^b	HOMO	HOMO- <i>n</i> (<i>n</i> = 0, 1, ...) (focusing on 3d MO)
Reference data	Experiment	CCSD(T) ^c	QSGW ^d	Experiment	Experiment
ω integration	Contour deformation ^e	Fully analytic	Fully analytic	Fully analytic	Fully analytic
QP equation	Linearization	Linearization	Spectral function	Linearization ^f & Spectral function ^g	Graphical solution & Spectral function
CBS limit	Not used (CN=4 only)	Not used (CN=4 only)	Not used (CN=3 only)	Not used (CN=2 only)	Used [see Eq. (34)] (CN=2,3,4,5)
Potential	ECP	AE	AE	PAW ^h	AE
RI	Used	Not used	Used	Not applicable ⁱ	Not used

^a The same set of molecules is used.^b For naphthalene only^c Ref. 4 showed that CCSD(T) with CN=4 causes an error of ~ 0.1 eV in the IE of small *sp* molecules with respect to experiment (the largest being 0.67 eV for NaCl).^d Ref. 46 showed that QSGW with CN=5 causes a mean absolute error of 0.18 eV in the IE of the first row atoms with respect to experiment (the largest being ~ 0.4 eV for O).^e Refs. 12 and 33 showed that the contour deformation technique produces almost the same *GW* self-energy as the fully analytic method for frontier and non-frontier orbitals, respectively.^f For 0% EXX^g For 100% EXX^h Projector-Augmented Waveⁱ GPAW uses augmented Wannier basis sets, whereas FIESTA, MOLGW, and TURBOMOLE use Gaussian basis sets.

D. Comparison with results in the literature

Some of our results for the performance of G_0W_0 starting-point and *evGW* self-consistency approaches in this work may seem to be at odds with some of the results in the literature. In this section, we discuss the origin of the apparent differences between them.

We begin with the G_0W_0 starting-point approach. Table IV summarizes a few results for the optimal amount of EXX in the G_0W_0 starting point in the literature. Interestingly, we see that there is a wide range of EXX amounts from 25% to 100%, and Refs. 4 and 22 obtained different results (50% and 100%, respectively) from the same set of molecules. It seems that 75% and 100% are too large compared to our results: 25–50%. One may guess that the large difference is due to implementation differences such as the basis type (e.g. Gaussian vs PW) and the frequency integration type (e.g. analytical vs numerical). However, Refs. 14 and 15 showed that such implementation differences have little effect on the G_0W_0 IE (~ 0.06 eV). There are a couple of other factors that have a stronger effect on G_0W_0 results than implementation differences. One factor is the choice of system and property. As we shown in Section IV A,

$G_0W_0@PBE\alpha(0.25 \leq \alpha \leq 1.00)$ IEs of *sp* systems are slightly different (by ~ 0.1 eV). Most existing G_0W_0 studies used the IE of *sp*-bonded systems to determine the optimal amount of EXX in the G_0W_0 starting point. The other factor is that the choice of QP equation solver and CBS extrapolation method. As we showed in Section III C 1 and Section III C 3, the linearization method and the CBS extrapolation method (e.g. whether to extrapolate or not and which fitting function and basis set to use for extrapolation) can cause a difference in the G_0W_0 IE on the order of ~ 0.1 eV. Overall, the combination of the two factors gives a large margin for the optimal amount of EXX in the G_0W_0 starting point, and thus is likely to produce the wide range of amounts that exist in the literature.

Next, we move on to the *evGW* self-consistency approach, and discuss the origin of apparently conflicting *evGW* results for IE and starting-point dependency. First, Ref. 7 reported that the G_nW_n approach with a local density approximation starting point gives good results for the IE of large *sp* molecules, whereas we found in Section IV B that $G_nW_n@PBE$ gives satisfactory results for the electronic structure (including the IE) of small 3d molecules. A comparison of computational details of Ref. 7 and this work is provided in the supple-

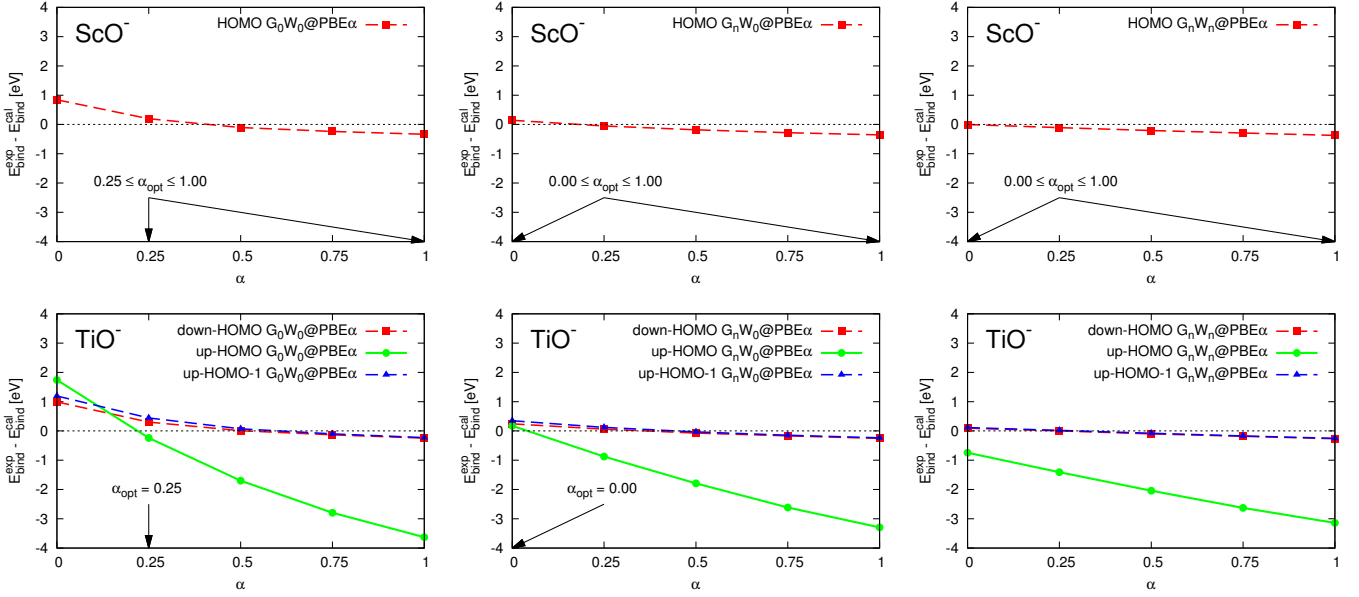


FIG. 8. (Color online) Effect of the GW starting point and the $evGW$ self-consistency level on the electronic structure of ScO^- and TiO^- . E_{bind}^{exp} and E_{bind}^{cal} represent experimental and calculated electron binding energies, respectively. Dashed and solid lines track sp - and d -electron binding energies, respectively. α_{opt} represents an optimal fraction of EXX in the GW starting point.

mentary material. We believe that the main origin of the different results is the orbital-character-dependent sensitivity of $evGW$ QP energies to a change in the $evGW$ self-consistency level. As we showed in Section IV B, $G_nW_0@PBE$ and $G_nW_n@PBE$ QP energies are slightly different for delocalized HOMO with weak $3d$ character by ~ 0.1 eV, but significantly different for localized HOMO with strong $3d$ character by ~ 1 eV. Different from this work, Ref. 7 used the linearization method, employed pseudopotentials and RI, and did not use the CBS limit, but these cause small (~ 0.1 eV) differences in the $evGW$ IEs, as shown in Section III C. Accordingly, they are most likely not the reason for the large (0.97 eV) difference between $G_nW_0@PBE$ and $G_nW_n@PBE$ IEs for CuO^- . Second, Ref. 40 reported that in water clusters, as the $evGW$ self-consistency level increases, the $evGW$ starting-point dependency decreases, whereas we found in Section III C 4 that in TMO anions, G_nW_n sometimes depends more strongly on the starting point than G_nW_0 . As mentioned in Section III C 4, we believe that the orbital character influences the $evGW$ starting-point dependency: for molecular orbitals with strong (weak) $3d$ character, G_nW_n depends more strongly (weakly) on the starting point than G_nW_0 . Overall, without molecular orbitals with strong $3d$ character (e.g. HOMO of CuO^-), our $evGW$ results for IE and starting-point dependency in this work are consistent with those in Refs. 7 and 40.

To verify our idea about the origin of the seemingly different results between this work and the literature, we performed a simple test: (i) we chose ScO^- and TiO^- as our analogs of sp molecules in the literature because their valence molecular orbitals have weak transition-metal

character, except for \uparrow -HOMO of TiO^- with entirely Ti $3d$ character, (ii) we applied 15 different starting-point-self-consistency hybrid GW schemes (G_0W_0 , G_nW_0 , and G_nW_n ; 0%, 25%, 50%, 75%, and 100% EXX) to them, and (iii) we searched for GW schemes that give a reasonably small error of less than 0.5 eV in the IE and the $3d$ -electron binding energy with respect to experiment. Fig. 8 shows the results of the test. We see that GW IEs of ScO^- and TiO^- (red dashed lines) depend weakly on the GW starting point and the $evGW$ self-consistency level, giving a large margin for the choice of GW schemes. 14 GW schemes out of 15 ($G_0W_0@PBE$ is an exception as expected) give a small error (less than 0.5 eV), which explains why there are a large number of different good GW schemes for the IE of sp molecules in the literature. We also see that the GW $3d$ -electron binding energy of TiO^- (green solid lines) depends strongly on the starting point and the self-consistency level, yielding a small margin for the choice of GW schemes. Only two GW schemes ($G_0W_0@PBE0$ and $G_nW_0@PBE$) out of 15 give a small error (less than 0.5 eV), which is why we obtained a small number of good GW schemes for the electronic structure of d molecules in this work. Overall, we confirm that evaluation results for the performance of GW schemes depend strongly on the choice of system and property (e.g. the IE with mainly sp character vs the electronic structure containing d states).

V. SUMMARY AND CONCLUSIONS

We calculated the electronic structure of closed- and open-shell molecular anions with partially and completely filled $3d$ shells using various levels of GW theory and compared calculated GW QP spectra to anion PES experiments to evaluate the performance of the GW approximation on both localized and delocalized states of small molecules containing $3d$ transition metals.

We found that the perturbative one-shot $G_0W_0@PBE$ scheme, which is the most widely used GW scheme for extended systems, has a couple of problems for finite systems. Fundamentally, $G_0W_0@PBE$ underestimates sp -electron and $3d$ -electron binding energies by ~ 1 eV and ~ 2 eV, respectively, which are considerably larger than the widely reported underestimation error of ~ 0.5 eV. Due to the non-uniform errors in the GW binding energy depending on the strength of $3d$ character of the molecular orbitals, $G_0W_0@PBE$ sometimes gives the incorrect orbital order. Practically, $G_0W_0@PBE$ suffers from the GW multi-solution issue due to the large distance between QP and gKS-PBE eigenvalues and the complicated pole (peak) structure in the self-energy (the spectral function).

We found that the starting-point approach, $G_0W_0@PBE\alpha$, can improve $G_0W_0@PBE$ at the expense of introducing a couple of problems. The G_0W_0 starting-point approach can give good sp - and $3d$ -electron binding energies at the same time, and thus, correct the wrong orbital order produced by PBE. Also, the G_0W_0 starting-point approach can avoid the GW multi-solution issue by reducing the distance between QP and gKS eigenvalues. However, the optimal amount of EXX in the G_0W_0 starting point strongly depends on the strength of $3d$ character of molecular orbitals, leading to the strong sensitivity of $3d$ -electron binding energy to a change in the EXX amount. That makes the optimal amount of EXX system- and property-dependent. More importantly, hybrid functionals frequently and randomly cause SCF convergence errors in open-shell systems, and thus require manual, time-consuming, and error-prone SCF convergence tests.

We found that the eigenvalue self-consistency approaches, $G_nW_0@PBE$ and $G_nW_n@PBE$, can improve $G_0W_0@PBE$, too. Especially, $G_nW_0@PBE$ not only gives as good sp - and $3d$ -electron binding energies as $G_0W_0@PBE\alpha$, but it also avoids the GW multi-solution issue of $G_0W_0@PBE$ and the SCF convergence issue of $G_0W_0@PBE\alpha$.

We recommend $G_nW_0@PBE$ because it offers practical advantages: (i) $G_nW_0@PBE$ is transferable, because it gives satisfactorily accurate results for both finite and extended systems, for both closed- and open-shell systems, and for both localized and delocalized states, (ii) $G_nW_0@PBE$ is predictive, because it does not need any system- and property-dependent parameters, and (iii) G_nW_0 is efficient, because it is free of tests to address SCF convergence and GW multi-solution issues

We attribute the good performance of $G_nW_0@PBE$ to the fortuitous cancellation effect: the overscreening of the Coulomb interaction due to the over-delocalized PBE wavefunction is cancelled by the underscreening due to the neglect of vertex corrections. In other words, for G_0W_0 applied to finite systems, PBE is a “bad” starting point in the sense that it causes a large (~ 1 – 2 eV) and orbital-character-dependent underestimation error in the electron binding energy, but for G_nW_0 applied to finite and extended systems, PBE is a “good” starting point in the sense that it accidentally produces the overscreening just as much as vertex corrections do, which is missing in self-consistent GW schemes.

Our results in this work – (i) $G_0W_0@PBE\alpha$ ($0.25 \leq \alpha \leq 0.50$) and $G_nW_0@PBE$ give good QP energies for localized and delocalized states of finite systems, and (ii) the $evGW$ starting-point dependency is more related to the orbital character than the self-consistency level – may at first sight seem to disagree with some results in the literature, but we argued that this is not the case upon further reflection. One reason for the seeming disagreement is that except for $G_0W_0@PBE\alpha$ ($0.00 \leq \alpha \leq 0.25$), the QP energy for HOMO of sp molecules depends weakly on the GW level and the starting point. The other reason is that except for $G_0W_0@PBE\alpha$ ($0.00 \leq \alpha \leq 0.25$), the change in the QP energy for HOMO of sp molecules from different GW levels and starting points is accidentally comparable to individual or combined errors (~ 0.1 eV) from multiple sources, such as the incomplete basis set (e.g. not only whether to extrapolate or not, but also which fitting function and basis set to use for extrapolation), the linearization method in G_0W_0 , and the insufficient number of eigenvalues to update in $evGW$.

$G_nW_0@PBE$ is not a conserving (in terms of particle number, momentum, and energy) and starting-point-independent GW scheme. It is not the most accurate or efficient GW scheme, either. However, for all the practical reasons summarized above, $G_nW_0@PBE$ gives satisfactory results at moderate computational costs for the electronic structure of small transition metal oxide systems, can be *seamlessly* applied to different systems and properties (e.g. molecular and periodic systems with and without d states), and thus is ideal for automated mass GW and BSE calculations for high-throughput screening and machine learning. Future studies on larger, more complex, and a wider range of transition metal oxide molecules are needed to further examine our findings and increase our understanding of GW methods applied to complex real systems.

ACKNOWLEDGMENTS

This work was supported by the U.S. Department of Energy Grant No. DE-SC0017824. The computation for this work was performed on the high performance computing infrastructure provided by Research Computing Support Services at the University of Missouri-Columbia.

This research also used resources of the National Energy Research Scientific Computing Center, a DOE Office of Science User Facility supported by the Office of Science of the U.S. Department of Energy under Contract No.

DE-AC02-05CH11231. We also would like to thank Bin Shi and Meisam Rezaei for useful discussions in the earlier stage of this work.

- ¹ F. Bruneval and M. Gatti, “Quasiparticle self-consistent gw method for the spectral properties of complex materials,” in *First Principles Approaches to Spectroscopic Properties of Complex Materials*, edited by C. Di Valentin, S. Botti, and M. Cococcioni (Springer Berlin Heidelberg, Berlin, Heidelberg, 2014) pp. 99–135.
- ² L. Reining, Wiley Interdisciplinary Reviews: Computational Molecular Science **8**, e1344 (2018), <https://onlinelibrary.wiley.com/doi/pdf/10.1002/wcms.1344>.
- ³ X. Ren, P. Rinke, V. Blum, J. Wieferink, A. Tkatchenko, A. Sanfilippo, K. Reuter, and M. Scheffler, New Journal of Physics **14**, 053020 (2012).
- ⁴ F. Bruneval and M. A. L. Marques, Journal of Chemical Theory and Computation **9**, 324 (2013), pMID: 26589035, <https://doi.org/10.1021/ct300835h>.
- ⁵ E. Pavarini, E. Koch, J. van den Brink, and G. Sawatzky, *Quantum Materials: Experiments and Theory*, Modeling and Simulation, Vol. 6 (Forschungszentrum Jlich, Jlich, 2016) p. 420 p.
- ⁶ F. Bruneval, T. Rangel, S. M. Hamed, M. Shao, C. Yang, and J. B. Neaton, Computer Physics Communications **208**, 149 (2016).
- ⁷ X. Blase, C. Attaccalite, and V. Olevano, Phys. Rev. B **83**, 115103 (2011).
- ⁸ M. J. van Setten, F. Weigend, and F. Evers, Journal of Chemical Theory and Computation **9**, 232 (2013), pMID: 26589026, <https://doi.org/10.1021/ct300648t>.
- ⁹ J. Wilhelm, M. Del Ben, and J. Hutter, Journal of Chemical Theory and Computation **12**, 3623 (2016), pMID: 27348184, <https://doi.org/10.1021/acs.jctc.6b00380>.
- ¹⁰ G. L. Gutsev, B. K. Rao, and P. Jena, The Journal of Physical Chemistry A **104**, 5374 (2000), <https://doi.org/10.1021/jp000384f>.
- ¹¹ J. M. Gonzales, R. A. King, and H. F. Schaefer, The Journal of Chemical Physics **113**, 567 (2000), <https://doi.org/10.1063/1.481832>.
- ¹² M. J. van Setten, F. Caruso, S. Sharifzadeh, X. Ren, M. Scheffler, F. Liu, J. Lischner, L. Lin, J. R. Deslippe, S. G. Louie, C. Yang, F. Weigend, J. B. Neaton, F. Evers, and P. Rinke, Journal of Chemical Theory and Computation **11**, 5665 (2015), pMID: 26642984, <https://doi.org/10.1021/acs.jctc.5b00453>.
- ¹³ F. Caruso, M. Dauth, M. J. van Setten, and P. Rinke, Journal of Chemical Theory and Computation **12**, 5076 (2016), pMID: 27631585, <https://doi.org/10.1021/acs.jctc.6b00774>.
- ¹⁴ E. Maggio, P. Liu, M. J. van Setten, and G. Kresse, Journal of Chemical Theory and Computation **13**, 635 (2017), pMID: 28094981, <https://doi.org/10.1021/acs.jctc.6b01150>.
- ¹⁵ M. Govoni and G. Galli, Journal of Chemical Theory and Computation **14**, 1895 (2018), pMID: 29397712, <https://doi.org/10.1021/acs.jctc.7b00952>.
- ¹⁶ M. Shishkin and G. Kresse, Phys. Rev. B **75**, 235102 (2007).
- ¹⁷ F. Fuchs, J. Furthmüller, F. Bechstedt, M. Shishkin, and G. Kresse, Phys. Rev. B **76**, 115109 (2007).
- ¹⁸ J. c. v. Klimeš, M. Kaltak, and G. Kresse, Phys. Rev. B **90**, 075125 (2014).
- ¹⁹ M. Grumet, P. Liu, M. Kaltak, J. c. v. Klimeš, and G. Kresse, Phys. Rev. B **98**, 155143 (2018).
- ²⁰ S. Körbel, P. Boulanger, I. Duchemin, X. Blase, M. A. L. Marques, and S. Botti, Journal of Chemical Theory and Computation **10**, 3934 (2014), pMID: 26588537, <https://doi.org/10.1021/ct5003658>.
- ²¹ F. Kaplan, M. E. Harding, C. Seiler, F. Weigend, F. Evers, and M. J. van Setten, Journal of Chemical Theory and Computation **12**, 2528 (2016), pMID: 27168352, <https://doi.org/10.1021/acs.jctc.5b01238>.
- ²² C. Rostgaard, K. W. Jacobsen, and K. S. Thygesen, Phys. Rev. B **81**, 085103 (2010).
- ²³ H. Wu and L.-S. Wang, The Journal of Physical Chemistry A **102**, 9129 (1998), <https://doi.org/10.1021/jp982588q>.
- ²⁴ H. Wu and L. Wang, The Journal of Chemical Physics **107**, 8221 (1997), <https://doi.org/10.1063/1.475026>.
- ²⁵ H. Wu, S. R. Desai, and L.-S. Wang, The Journal of Physical Chemistry A **101**, 2103 (1997), <https://doi.org/10.1021/jp9631442>.
- ²⁶ V. D. Moravec, S. A. Klopčič, B. Chatterjee, and C. C. Jarrold, Chemical Physics Letters **341**, 313 (2001).
- ²⁷ F. Bruneval, N. Vast, L. Reining, M. Izquierdo, F. Sirotti, and N. Barrett, Phys. Rev. Lett. **97**, 267601 (2006).
- ²⁸ L. Y. Isseroff and E. A. Carter, Phys. Rev. B **85**, 235142 (2012).
- ²⁹ M. L. Tiago and J. R. Chelikowsky, Phys. Rev. B **73**, 205334 (2006).
- ³⁰ A. Seidl, A. Görling, P. Vogl, J. A. Majewski, and M. Levy, Phys. Rev. B **53**, 3764 (1996).
- ³¹ Y.-M. Byun and C. A. Ullrich, Computation **5**, 9 (2017).
- ³² T. Sander, E. Maggio, and G. Kresse, Phys. Rev. B **92**, 045209 (2015).
- ³³ D. Golze, J. Wilhelm, M. J. van Setten, and P. Rinke, Journal of Chemical Theory and Computation **14**, 4856 (2018), pMID: 30092140, <https://doi.org/10.1021/acs.jctc.8b00458>.
- ³⁴ A. J. Cohen, D. J. Tozer, and N. C. Handy, The Journal of Chemical Physics **126**, 214104 (2007), <https://doi.org/10.1063/1.2737773>.
- ³⁵ A. S. Menon and L. Radom, The Journal of Physical Chemistry A **112**, 13225 (2008), pMID: 18759419, <https://doi.org/10.1021/jp803064k>.
- ³⁶ J. G. Hill and J. A. Platts, The Journal of Chemical Physics **128**, 044104 (2008), <https://doi.org/10.1063/1.2826348>.
- ³⁷ J. G. Hill and K. A. Peterson, Journal of Chemical Theory and Computation **8**, 518 (2012), <https://doi.org/10.1021/ct200856f>.
- ³⁸ M. S. Hybertsen and S. G. Louie, Phys. Rev. B **34**, 5390 (1986).
- ³⁹ T. Kotani, M. van Schilfgaarde, and S. V. Faleev, Phys.

- Rev. B **76**, 165106 (2007).
- ⁴⁰ X. Blase, P. Boulanger, F. Bruneval, M. Fernandez-Serra, and I. Duchemin, *The Journal of Chemical Physics* **144**, 034109 (2016), <https://doi.org/10.1063/1.4940139>.
 - ⁴¹ C. Hättig, W. Klopper, A. Köhn, and D. P. Tew, *Chemical Reviews* **112**, 4 (2012), pMID: 22206503, <https://doi.org/10.1021/cr200168z>.
 - ⁴² F. Hüsler, T. Olsen, and K. S. Thygesen, *Phys. Rev. B* **87**, 235132 (2013).
 - ⁴³ T. Rangel, S. M. Hamed, F. Bruneval, and J. B. Neaton, *Journal of Chemical Theory and Computation* **12**, 2834 (2016), pMID: 27123935, <https://doi.org/10.1021/acs.jctc.6b00163>.
 - ⁴⁴ L. Hung, F. Bruneval, K. Baishya, and S. Ögüt, *Journal of Chemical Theory and Computation* **13**, 2135 (2017), pMID: 28387124, <https://doi.org/10.1021/acs.jctc.7b00123>.
 - ⁴⁵ B. Shi, S. Weissman, F. Bruneval, L. Kronik, and S. Ögüt, *The Journal of Chemical Physics* **149**, 064306 (2018), <https://doi.org/10.1063/1.5038744>.
 - ⁴⁶ F. Bruneval, *The Journal of Chemical Physics* **136**, 194107 (2012), <https://doi.org/10.1063/1.4718428>.
 - ⁴⁷ L. Hung, F. Bruneval, K. Baishya, and S. Ögüt, *Journal of Chemical Theory and Computation* **13**, 5820 (2017), pMID: 29099593, <https://doi.org/10.1021/acs.jctc.7b01054>.
 - ⁴⁸ P. Koval, D. Foerster, and D. Sánchez-Portal, *Phys. Rev. B* **89**, 155417 (2014).
 - ⁴⁹ P. Liao and E. A. Carter, *Phys. Chem. Chem. Phys.* **13**, 15189 (2011).
 - ⁵⁰ K. Momma and F. Izumi, *Journal of Applied Crystallography* **41**, 653 (2008), <https://onlinelibrary.wiley.com/doi/pdf/10.1107/S0021889808012016>.
 - ⁵¹ B. Dai, K. Deng, J. Yang, and Q. Zhu, *The Journal of Chemical Physics* **118**, 9608 (2003), <https://doi.org/10.1063/1.1570811>.
 - ⁵² A. J. Bridgeman and J. Rothery, *J. Chem. Soc., Dalton Trans.*, 211 (2000).
 - ⁵³ E. Miliordos and A. Mavridis, *The Journal of Physical Chemistry A* **114**, 8536 (2010), pMID: 20113002, <https://doi.org/10.1021/jp910218u>.
 - ⁵⁴ C. W. Bauschlicher and H. Partridge, *The Journal of Chemical Physics* **109**, 8430 (1998), <https://doi.org/10.1063/1.477506>.
 - ⁵⁵ M. B. Walsh, R. A. King, and H. F. Schaefer, *The Journal of Chemical Physics* **110**, 5224 (1999), <https://doi.org/10.1063/1.478418>.
 - ⁵⁶ H. Xian, Z. Cao, X. Xu, X. Lu, and Q. Zhang, *Chemical Physics Letters* **326**, 485 (2000).
 - ⁵⁷ A. Daoudi, A. T. Benjelloun, J. Flament, and G. Berthier, *Journal of Molecular Spectroscopy* **194**, 8 (1999).
 - ⁵⁸ P. S. Bagus, C. J. Nelin, and C. W. Bauschlicher, *The Journal of Chemical Physics* **79**, 2975 (1983), <https://doi.org/10.1063/1.446126>.
 - ⁵⁹ Y. Lefebvre, B. Pinchemel, J. M. Delaval, and J. Schamps, *Physica Scripta* **25**, 329 (1982).
 - ⁶⁰ G. L. Gutsev, L. Andrews, and C. W. Bauschlicher, Jr., *Theoretical Chemistry Accounts* **109**, 298 (2003).
 - ⁶¹ C. A. Fancher, H. L. de Clercq, O. C. Thomas, D. W. Robinson, and K. H. Bowen, *The Journal of Chemical Physics* **109**, 8426 (1998), <https://doi.org/10.1063/1.477505>.
 - ⁶² M. Strange, C. Rostgaard, H. Häkkinen, and K. S. Thygesen, *Phys. Rev. B* **83**, 115108 (2011).